Reorientational relaxation of a linear probe molecule in a simple glassy liquid

W. Götze, A. P. Singh, and Th. Voigtmann
Physik-Department, Technische Universität München, 85747 Garching, Germany
(Received 29 December 1999)

Within the mode-coupling theory (MCT) for the evolution of structural relaxation in glass-forming liquids, correlation functions and susceptibility spectra are calculated characterizing the rotational dynamics of a top-down symmetric dumbbell molecule, consisting of two fused hard spheres immersed in a hard-sphere system. It is found that for sufficiently large dumbbell elongations, the dynamics of the probe molecule follows the same universal glass-transition scenario as known from the MCT results of simple liquids. The α-relaxation process of the angular-index $j=1$ response is stronger, slower, and less stretched than the one for $j=2$, in qualitative agreement with results found by dielectric-loss and depolarized-light-scattering spectroscopy for some supercooled liquids. For sufficiently small elongations, the reorientational relaxation occurs via large-angle flips, and the standard scenario for the glass-transition dynamics is modified for odd-j responses due to precursor phenomena of a nearby type-A MCT transition. In this case, a major part of the relaxation outside the transient regime is described qualitatively by the β-relaxation scaling laws, while the α-relaxation scaling law is strongly disturbed.

PACS number(s): 64.70.Pf, 61.20.Lc, 61.25.Em

I. INTRODUCTION

During the past ten years, the evolution of structural relaxation in glass-forming liquids has been intensively studied using neutron-scattering spectroscopy, various light-scattering techniques, dielectric-loss spectroscopy, and molecular-dynamics simulation. Results of this work have also been used to test the mode-coupling theory (MCT), which interprets the structural relaxation as precursor of the glass transition. Originally, the MCT was proposed as an approximation approach for the cage effect in liquids [1,2]. In its simplest version, the MCT equations of motion describe an ideal liquid-to-glass transition, i.e., a bifurcation from ergodic to nonergodic dynamics, if control parameters like temperature T or packing fraction φ cross critical values T_c or φ_c, respectively. This bifurcation is connected with the evolution of a two-step relaxation scenario entirely determined by the regularly changing equilibrium structure. Two divergent time scales appear, closely connected to two power-law decay processes. A detailed description of these results can be found in Ref. [3] and references therein. Comparisons of the theoretical results for simple model systems with experiments done on colloids [4,5], and with computer-simulation studies [6,7] demonstrate the validity of the microscopic MCT approach. For the solutions of the MCT equations, a variety of results has been derived by asymptotic expansions, using as a small parameter the distance from the critical point, $\epsilon=(\varphi-\varphi_c)/\varphi_c$, or $\epsilon=(T_c-T)/T_c$, respectively. The leading-order results of this expansion establish universality features of the MCT dynamics. Assessments of the theory have been reached by comparing spectra in the GHz regime or relaxation curves within the picosecond window with the universal results. The outcome of this work, which is reviewed in Ref. [8], leads to the conclusion that MCT properly describes some essential features of structural relaxation even for some complicated molecular liquids.

The MCT for simple systems has been extended recently to liquids of nonspherical molecules [9–11]. But so far, only the bifurcation equation for the so-called nonergodicity parameters resulting within the new theory could be solved. Comparing these results with the findings of molecular-dynamics simulations for a liquid of linear molecules [12,13] and for water [11] indicates that the MCT for molecular liquids is promising. It was also predicted that there can be two states of nonergodic motion for nonspherical molecules. These states are connected by a type-A transition if the molecules exhibit a top-down symmetry [9,10,14]. Such transitions are generic possibilities in MCT, provided there is some symmetry in the problem rendering certain mode-coupling coefficients zero [15]. At a type-A transition, the nonergodicity parameters change continuously, whereas at the conventional MCT transition, referred to in this context as a type-B transition, a discontinuity occurs [16].

In this paper, correlation functions and susceptibility spectra shall be discussed, which deal with the glassy dynamics of the orientational degrees of freedom of nonspherical molecules. The results are obtained as solutions of the equations of motion derived previously [10] for the dynamics of a linear probe molecule immersed in a simple liquid. A top-down symmetric dumbbell of two fused hard spheres will be considered as the molecule, and as the solute, a hard-sphere system is chosen. This model deals with the simplest problem concerning glassy rotational dynamics, namely, the influence of the cages formed by the neighbors of the molecule on the molecule's reorientational motion as it is caused by steric hindrance. The dynamics will be exemplified for two cases: a molecule with a large elongation and a molecule with a small elongation.

It will be shown that large elongations lead to strong coupling of the rotational degrees of freedom to the density fluctuations of the solute, such that the glassy dynamics of the latter enforces the validity of all the universal MCT laws for the solvent. Moreover, the corrections to the leading-order-asymptotic laws show the same qualitative trends as studied for simple liquids [17,18]. A motivation of the present study

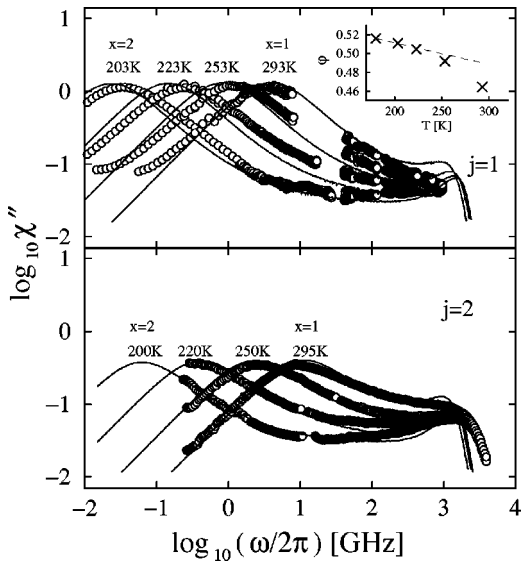

FIG. 1. Susceptibility spectra χ'' of propylene carbonate (PC, symbols) and solutions obtained for a symmetric hard-sphere dumbbell with elongation $\zeta=0.80$ immersed in a hard-sphere solvent (full lines, see text for details). The symbols represent dielectric-loss spectra measured by Schneider *et al.* [19] (upper panel) and depolarized-light-scattering spectra of Du *et al.* [20] (lower panel) for temperatures as indicated. The full lines are calculated for the distance parameter $\epsilon=(\varphi-\varphi_c)/\varphi_c=-10^{-x}$ with $x=1$, 1.33, 1.67, and 2 for angular momentum index $j=1$ and 2, respectively. Computed frequencies have been rescaled by a factor of 10 to meet the experimental GHz scale. The calculated susceptibilities have been divided by 2.8 for the $j=1$ case in order to normalize the spectra at $\omega/2\pi=2$ GHz. The inset exhibits packing fraction φ vs temperature T for which the spectra are fitted. Here, the critical value of the hard-sphere system, $\varphi_c=0.516$, corresponding to the critical temperature of PC, $T_c\approx 180$ K, was added. The dashed line demonstrates the extrapolation from the found φ-T mapping to T_c.

is the explanation of three general properties of the α relaxation in molecular liquids, which are exhibited in Fig. 1. In this figure, experimental susceptibility spectra for the van der Waals liquid propylene carbonate (PC) are reproduced for four temperatures. One set of data deals with the response for angular-momentum index $j=1$; it was obtained by dielectric-loss spectroscopy [19]. The other set was measured by depolarized-light-scattering spectroscopy [20] and deals with the $(j=2)$ reorientational dynamics. The data show for $T=293$ K and $T=295$ K α-relaxation peaks at 4 GHz $(j=1)$ and 10 GHz $(j=2)$, respectively. These temperatures exceed the melting temperature $T_m=218$ K of PC by more than 70 K. Lowering T to 200 K, the α peaks of the spectra are shifted down by about two orders of magnitude. The shape of the α peak is temperature independent, and the ratio of the α-process-time scales, characterizing the α-peak-maximum positions for the two values of j, is also T independent. These are two features that MCT predicts to be universal. The first nonuniversal feature to be understood is, that the α-peak intensity, taken relative to that of the band of microscopic excitations at around 1 THz, is larger for the $(j=1)$ response than for the $(j=2)$ case: the former exceeds the latter by about a factor of 2.7. Second, the $(j=1)$ response is slower than the response for $j=2$: the ratio of the α-peak positions is about 2.5. Third, the α peak of the $(j=1)$ response is less stretched than the peak for $j=2$, i.e., the half-width of the $(j=1)$ peak is smaller than that of the $(j=2)$ peak. If one describes these peaks by the spectra of the Kohlrausch law, $\Phi(t)\propto e^{-(t/\tau)^\beta}$, the stretching exponent β for $j=1$, $\beta_{j=1}\approx 0.9$ [19] is larger than the one for $j=2$, $\beta_{j=2}\approx 0.8$ [20]. The same three α-peak features are noticed, if one compares the depolarized-light-scattering spectra of glycerol [21] with the corresponding dielectric-loss spectra [22]. A fourth general feature to be explained is the large ratio of the α-relaxation-time scale found by depolarized-light-scattering spectroscopy and the one found for the longitudinal elastic modulus by Brillouin-scattering spectroscopy. For Salol, a ratio of about 10 was reported [23], while for PC, a factor of about 5 was found [20].

The small elongation of concern in this paper is chosen so that it exceeds the critical value for the above-mentioned type-A transition by about 10%. The theory for the corrections to the leading-order asymptotic laws [17,18] implies that these diverge at a type-A transition. Therefore, the range of validity of the universality features of the standard MCT bifurcation shrinks upon approaching the type-A transition. It will be shown that in our example the standard results are not exhibited any more for reasonable choices of the distance parameter ϵ. In particular, it is impossible to identify a two-step scenario for the odd-l correlators, nor is α-relaxation scaling observed.

The paper is organized as follows. In Sec. II, the model is defined, and the MCT equations are noted. After an overview of the general scenario for the evolution of the glassy relaxation of the reorientational correlators (Sec. III A), the differences between the relaxation patterns for the $(j=1)$ and $(j=2)$ response are described for strong (Sec. III B) and weak (Sec. III C) steric hindrance. In Sec. III D it is demonstrated how the β relaxation is described by the first scaling law, and in Sec. III E it is discussed how the α-relaxation scaling-law description emerges. The concluding Sec. IV summarizes the results.

II. THE MODEL SYSTEM

A. The solvent

A system of N spherical particles shall be considered as the solvent. The basic variables describing the structure are the density fluctuations for the wave vector $\vec{q}$: $\varrho_{\vec{q}}=\Sigma_\kappa \exp(i\vec{q}\cdot\vec{r}^{\,\kappa})/\sqrt{N}$. Here $\vec{r}^{\,\kappa}, \kappa=1,2,\ldots,N$, labels the centers of the particles. The structure factor $S_q=\langle|\varrho_{\vec{q}}|^2\rangle$ provides the simplest information on the equilibrium distribution of the particles; here, $\langle\ \rangle$ denotes canonical averaging. Because of rotational symmetry, S_q depends on the wave-vector modulus $q=|\vec{q}|$ only. The structure factor can be expressed through the direct correlation function c_q via the Ornstein-Zernicke equation $S_q=1/(1-\rho c_q)$, where ρ denotes the particle density [24]. The simplest quantities, characterizing the structural dynamics in a statistical manner, are the normalized autocorrelation functions for the density fluctuations, called the density correlators $\Phi_q(t)=\langle\varrho_{\vec{q}}(t)^*\varrho_{\vec{q}}\rangle/S_q$. The evolution with increasing time t is given by the canonical equations of motion. We will also need Fourier-Laplace transforms for complex frequency z, $\mathrm{Im}\, z\geq 0$, $\Phi_q(z)$, using the convention: $F(z)$

$=\mathrm{i}\int_0^\infty \exp(\mathrm{i}zt)F(t)dt$. For real frequency ω, one gets with $z=\omega+i0$: $F(z)=F'(\omega)+iF''(\omega)$. The imaginary part $F''(\omega)$ is called the fluctuation spectrum, and $\chi''(\omega)=\omega F''(\omega)$ is the susceptibility spectrum [24].

The basic version of MCT consists of two equations [2]. The first one is exact and derived within the Zwanzig-Mori formalism:

$$\partial_t^2\Phi_q(t)+\Omega_q^2\Phi_q(t)+\Omega_q^2\int_0^t m_q(t-t')\ \partial_{t'}\Phi_q(t')dt'=0. \tag{1a}$$

Here, $\Omega_q=vq/\sqrt{S_q}$, with v denoting the thermal velocity. The relaxation kernel $m_q(t)$ is a fluctuating-force correlator. The equation has to be solved with the initial condition $\Phi_q(t)=1-(\Omega_q t)^2/2+\mathcal{O}(t^3)$ [24]. Equation (1a) is equivalent to the double fraction

$$\Phi_q(z)=\frac{-1}{z-\dfrac{\Omega_q^2}{z+\Omega_q^2\ m_q(z)}}. \tag{1b}$$

The second MCT equation is obtained by writing the kernel as a sum of a regular term and a contribution describing the cage effect. The latter is treated by Kawasaki's factorization approximation for the force correlations. It is found to be a quadratic functional of the density fluctuations: $\Sigma_{\vec{k}+\vec{p}=\vec{q}}\ V(\vec{q},\vec{k},\vec{p})\,\Phi_k(t)\,\Phi_p(t)$. For the sake of simplicity, the regular term shall be neglected in the following. Furthermore, the wave-vector modulus will be discretized to M values with equal spacing h. Thus, q, k, p can be considered as labels running from 1 to M. As a result, the kernel is given as a quadratic mode-coupling polynomial $\mathcal{F}_q$ of the M correlators $\Phi_q(t)$, $q=1,\ldots,M$:

$$m_q(t)=\mathcal{F}_q[\Phi_k(t)]=\sum_{kp} V_{qkp}\,\Phi_k(t)\,\Phi_p(t). \tag{2}$$

The positive coupling coefficients V_{qkp} are given by S_q and c_q [17]. Anticipating these equilibrium quantities to be known, Eqs. (1a) and (2) are closed.

Equations (1) and (2) exhibit a transition from liquid-state dynamics in the regime $T>T_c$ or $\varphi<\varphi_c$ to glass-state dynamics for $T\leqslant T_c$ or $\varphi\geqslant\varphi_c$. In the former regime the density fluctuations decay to zero for long times, $\Phi_q(t\to\infty)=0$. The ideal glass states exhibit a nontrivial long-time limit, which is called the nonergodicity parameter, $f_q=\Phi_q(t\to\infty)>0$. It is the Debye-Waller factor of the glass. At the transition, this long-time limit is discontinuous, and the jump is called a critical nonergodicity parameter or plateau, $f_q^c=f_q(T\nearrow T_c,\varphi\searrow\varphi_c)>0$. At the critical point, the correlators decay algebraically: $\Phi_q(t)=f_q^c+h_q(t/t_0)^{-a}+\mathcal{O}((t/t_0)^{-2a})$. The exponent a, $0<a<1/2$, is called the critical exponent, and $h_q>0$ is denoted as the critical amplitude. t_0 marks the time scale of the transient from the microscopic motion to the relaxation dynamics of the MCT. The MCT α process is defined as the dynamics for those times, where the correlators of the liquid decay from the plateau f_q^c to zero. The MCT β process deals with the dynamics, where the correlators are near the plateau, i.e., $|\Phi_q(t)-f_q^c|\ll 1$. The first relaxation step of the anomalous dynamics is given by the initial part of the β process; it deals with the decay towards the plateau for times outside the transient: $(t/t_0)\gg 1$, $\Phi_q(t)\geqslant f_q^c$. The second step is the α decay in the liquid. Its initial part is identical with the final part of the β process, and it follows von Schweidler's law $\Phi_q(t)-f_q^c\propto -h_q t^b$. The exponent b, $0<b\leqslant 1$, is called the von Schweidler exponent.

In a leading-order expansion in the small parameter $|\Phi_q(t)-f_q^c|$ one finds the universal results for the β process. There holds the factorization theorem

$$\Phi_q(t)-f_q^c=h_q G(t). \tag{3}$$

The dependence on time and on control parameters is given by the q-independent function $G(t)$, which is called the β correlator. It is determined by the equation

$$\sigma-\lambda G(t)^2=\frac{d}{dt}\int_0^t G(t-t')G(t')dt', \tag{4}$$

to be solved with the initial condition $G(t\to 0)=(t/t_0)^{-a}+\mathcal{O}(t^a)$. The number λ, $0<\lambda<1$, is referred to as the exponent parameter. σ is a smooth function of the control parameters and is called the separation parameter. Its zero defines the critical point. Expanding in leading order in the distance ϵ, one can write $\sigma=C\epsilon$, $C>0$.

From Eq. (4), one derives the first scaling law

$$G(t)=c_\sigma g_\pm(\hat{t}),\ \epsilon\gtrless 0 \quad \hat{t}=t/t_\sigma. \tag{5}$$

Here, $c_\sigma=\sqrt{|\sigma|}$ denotes the amplitude scale, and t_σ abbreviates the first characteristic time scale of the MCT-transition scenario:

$$t_\sigma=t_0/|\sigma|^{1/2a}. \tag{6a}$$

The master functions $g_\pm(\hat{t})$ are determined by λ as solutions of Eq. (4) for $\sigma=\pm 1$, respectively. They interpolate monotonously between $g_\pm(\hat{t}\ll 1)=\hat{t}^{-a}$ and $g_+(\hat{t}\gg 1)=1/\sqrt{1-\lambda}$ or $g_-(\hat{t}\gg 1)=-B\hat{t}^b$. von Schweidler's law is obtained as the long-time limit on the scale t_σ in the form: $\Phi_q(t)=f_q^c-h_q(t/t'_\sigma)^b$. Here t'_σ abbreviates the second characteristic scale of the theory:

$$t'_\sigma=B^{-1/b}t_0/|\sigma|^\gamma, \quad \gamma=(1/2a)+(1/2b). \tag{6b}$$

The α process obeys for $\epsilon\to 0$ the second scaling law, called the superposition principle,

$$\Phi_q(t)=\tilde{\Phi}_q(\tilde{t}), \quad \tilde{t}=t/t'_\sigma. \tag{7}$$

The control-parameter-independent master function $\tilde{\Phi}_q(\tilde{t})$ exhibits the initial decay $\tilde{\Phi}_q(\tilde{t})=f_q^c-h_q\tilde{t}^b+\mathcal{O}(\tilde{t}^{2b})$. The parameters f_q^c, h_q, and λ are determined by $\mathcal{F}_q$ from Eq. (2) for control parameters at the critical point. The same holds for the function $\tilde{\Phi}_q(\tilde{t})$. The constant C is determined by the first Taylor coefficient in ϵ of the deviations of $\mathcal{F}_q$ from its value at the critical point. Formulas for these quantities can be found in Ref. [16], where also the original work is cited. The theory for the leading corrections to the quoted results has been worked out in Ref. [17].

The calculations in this paper will be done for the hard-sphere system (HSS). The temperature does not enter the structure, but determines the time scale via the thermal velocity only: $v^2 \propto T$. The relevant control parameter is the packing fraction: $\varphi = \pi(\rho d^3)/6$, where d is the particle diameter. The structure factor will be calculated within the Percus-Yevick theory [24]. The discretization will be done for $M = 100$ wave-vector values with step size $hd = 0.4$. For this model, all the mentioned MCT quantities have been reported in Ref. [17]. In particular it was found $\varphi_c = 0.516$, $C = 1.54$,

$$\lambda = 0.735, \quad a = 0.312, \quad b = 0.583, \quad \gamma = 2.46, \quad B = 0.836. \tag{8}$$

The results for the glass transition of the HSS are documented comprehensively in Refs. [17,18], albeit for a Brownian microscopic dynamics. The bifurcation scenario for the model with Newtonian dynamics as defined by Eqs. (1) and (2) is demonstrated for the wave vector $q = 10.6/d$ in Ref. [25], where the transient time scale was determined $t_0 = 0.0236(d/v)$. For the presentation of our results in the following figures, the units of length and time will be chosen so that $d = 1$ and $d/v = 1$. The control parameters φ shall be cited by the logarithm x of the distance parameter ϵ:

$$(\varphi - \varphi_c)/\varphi_c = \epsilon = \pm 10^{-x}. \tag{9}$$

As in the previous work [17,18,25], the MCT equations are solved in the time domain. The solutions are then Laplace transformed to get $\Phi'_q(\omega) + i\Phi''_q(\omega)$. Similarly, the transformed kernel $m'_q(\omega) + im''_q(\omega)$ is calculated from $m_q(t)$ in Eq. (2). These results are used to compare the left-hand side of Eq. (1b) with the right-hand side. Thereby a verification of the numerical solutions is obtained.

B. The solute

As a model for a dilute solution of molecules we shall consider a single linear molecule immersed in a simple system. The position of this molecule is described by the tensor-density fluctuations $\varrho_j^\nu(\vec{q}) = R_j^\nu(\vec{e})\exp(i\vec{q}\cdot\vec{r})$. Here, $\vec{r}$ denotes the center-of-mass position and $\vec{e}$ abbreviates the axis of the molecule. The R_j^ν are related to the spherical harmonics by: $R_j^\nu(\vec{e}) = i^j\sqrt{4\pi}\ \mathrm{Y}_j^\nu(\vec{e})$. The solute-solvent equilibrium correlations are described by the generalized structure factors $S_J(q) = \langle \varrho^*(\vec{q}_0)\varrho_J^0(\vec{q}_0)\rangle$, where $\vec{q}_0 = (0,0,q)$. The proper generalization of the density correlators for simple systems are tensor-density correlators for the molecule, $\langle \varrho_i^\mu(\vec{q}_0,t)^*\varrho_j^\mu(\vec{q}_0)\rangle$. The MCT for these quantities shall be simplified by restricting the correlators to the diagonal elements

$$\Phi(qj\mu,t) = \langle \varrho_j^\mu(\vec{q}_0,t)^*\varrho_j^\mu(\vec{q}_0)\rangle. \tag{10}$$

Correlation functions for wave vectors $\vec{q}$ different from $\vec{q}_0$ can be obtained from the specified ones by elementary transformations [10].

The first equation of the MCT for the molecule dynamics reads [10]:

$$\Phi(qj\mu,z) = \frac{-1}{z - \dfrac{\Omega_{Tq}^2}{z + \Omega_{Tq}^2(q)m_T(qj\mu,z)} - \dfrac{\Omega_{Rj}^2}{z + \Omega_{Rj}^2 m_R(qj\mu,z)}}. \tag{11}$$

Here, $\Omega_{T,q} = vq$ is the characteristic frequency for the translational motion of a tagged particle. $\Omega_{R,j} = v_R\sqrt{j(j+1)}$ is the analog for the rotational dynamics, where $j(j+1)$ plays here and in the following a similar role as q^2 for the translational motion. The frequency v_R denotes the thermal velocity for the rotation. The relaxation kernels m_T and m_R are approximated along the same lines as indicated above for simple systems. They are obtained as a functional of the density correlators of the solvent, multiplied by the tensor-density correlators of the solute [10]. Let us discretize the wave vector to, say, M' values with equal spacing h'. Let us also restrict the angular-momentum index by some upper cutoff value l_{co}. One obtains the kernels as mode-coupling polynomials

$$\begin{aligned} m_\alpha(qj\mu,t) &= \mathcal{F}_{\alpha qj\mu}[\Phi(kl\nu,t),\Phi_p(t)] \\ &= \sum_{kpl\nu} V_{\alpha qj\mu}(kpl\nu)\Phi(kl\nu,t)\Phi_p(t), \\ \alpha &= R,T. \end{aligned} \tag{12}$$

The positive coefficients $V_{\alpha qj\mu}(kpl\nu)$, $j,l = 0,1,\ldots,l_{co}$ are given in Ref. [26] as a specialization of the results in Ref. [10]. They are expressed in terms of S_q and $S_J(q)$ for $J = 0,1,\ldots,2l_{co}$. Anticipating S_q, $S_J(q)$, and $\Phi_q(t)$ as known, Eqs. (11) and (12) are closed equations for the determination of the $M'(l_{co}+1)^2$ correlators $\Phi(qj\mu,t)$.

The quantities of main interest for a statistical description of the rotation of the molecule are the reorientational correlators, defined with the Legendre polynomials P_j:

$$C^{(j)}(t) = \langle \mathrm{P}_j(\vec{e}(t)\cdot\vec{e})\rangle, \quad j = 1,2,\ldots. \tag{13a}$$

They are the long-wavelength limits of the general correlators; $\Phi(q\to 0\ j0,t) = C^{(j)}(t)$ [10]. One gets from Eq. (11) the fraction representation in analogy to Eq. (1b):

$$C^{(j)}(z) = \frac{-1}{z - \dfrac{\Omega_{Rj}^2}{z + \Omega_{Rj}^2\ m_j^R(z)}}. \tag{13b}$$

Here the kernel $m_j^R(z)$ is the $q \to 0$ limit of $m_R(qj0,t)$. Carrying out the limit in the general formula for $m_R(qj0,t)$ [10] and discretizing the wave-vector integral afterwards, one finds:

$$m_j^R(t) = \mathcal{F}[\Phi(kj\mu,t),\Phi_k(t)] = \sum_{jkl\nu} V_{kl\nu}^j \; \Phi(kl\nu,t)\Phi_k(t). \tag{14}$$

The positive coupling coefficients $V_{kl\nu}^j$ are listed in Ref. [26]. After evaluation of $\Phi(kl\nu,t)$ and $\Phi_k(t)$ the correlators for the M' values of k, Eq. (14) yields the kernel $m_j^R(t)$. Fourier-Laplace transformation gives $m_j^R(z)$ and Eq. (13b) provides $C^{(j)}(z)$. Fourier-cosine transformation of the spectrum $C^{(j)''}(\omega)$ leads to $C^{(j)}(t)$.

The theory shall be applied for a dumbbell consisting of two equal fused hard spheres of diameter d and distance ζd between the centers. Thus, besides the packing fraction φ, there is the elongation parameter ζ as the second control parameter specifying the structure. The structure factor $S_J(q)$ and the corresponding pair correlation functions $g_J(r)$ are evaluated within the Percus-Yevick theory [27]. Figure 2 exhibits the probability distribution to find a solvent particle in the plane through the symmetry axis of the dumbbell. The upper panel, calculated for $\zeta = 0.80$, shows a pronounced quadrupolar pattern extending over several shells. For the small elongation $\zeta = 0.33$, the lower panel shows that anisotropy is almost lost from the third shell onwards. The calculations of the dynamics will be done for such moment of inertia that $v_R/d = \sqrt{2}v/d$. The discretization will be done with $M' = 50$ wave vectors with spacing $h' = 0.8$. The cutoff for the angular-momentum index is chosen as $l_{lo} = 7$ for $\zeta = 0.80$ and $l_{lo} = 5$ for $\zeta = 0.33$. The equation of motion (11) is transformed to an integrodifferential equation in analogy to Eq. (1a) and then solved by an algorithm similar to that used for the standard MCT problem [26].

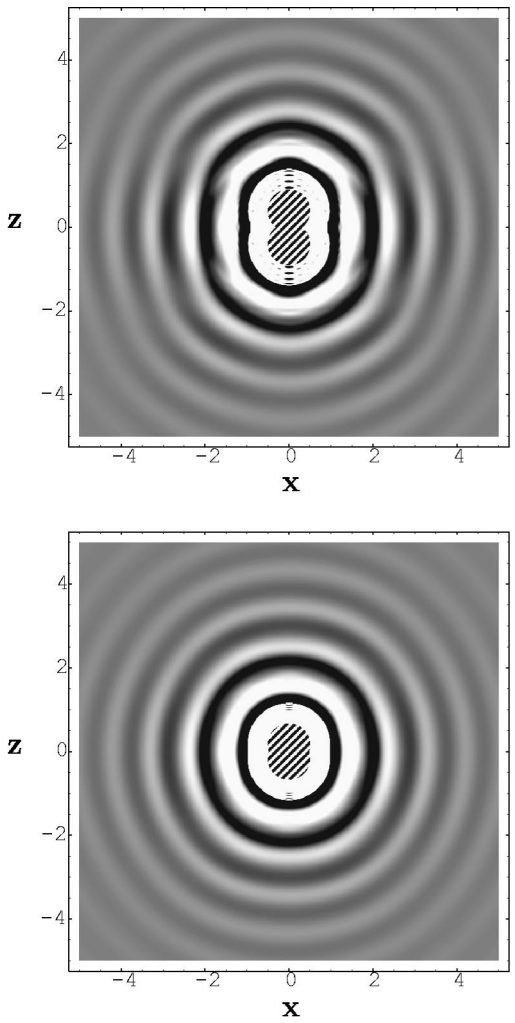

FIG. 2. Angular-dependent solute-solvent pair-distribution function $g(\vec{r},\vec{\Omega})$, calculated within the Percus-Yevick theory, for a top-down symmetric solute molecule consisting of two equal fused hard spheres with elongation $\zeta = 0.8$ (upper panel) and $\zeta = 0.33$ (lower panel). The shown $x-z$ plane contains the molecule axis. Grey corresponds to $g(\vec{r},\vec{\Omega}) \approx 1$, dark and white areas show regions with higher and lower probability to find a solvent particle, respectively. The cut through the dumbbell is shown hatched. The diameter d of each sphere is chosen to match that of the surrounding solvent particles. The unit of length is chosen here and in all following figures such that $d = 1$. The packing fraction of the hard-sphere solvent is at the critical value $\varphi_c = 0.516$. $g(\vec{r},\vec{\Omega})$ was approximated using a Legendre-polynomial expansion with angular-momentum indices up to $j = 16$.

III. RESULTS

A. General features of reorientational relaxation

Figure 3 demonstrates the transition scenario for the solute correlators for two representative wave vectors q and three values of the angular momentum index j. The calculated correlators exhibit a very weak dependence on the helicity index μ, and therefore only the solutions for $\mu = 0$ are shown. The wave vector $q = 7.0$ is close to the structure-factor-peak position, and $q = 10.6$ is near the first minimum of S_q. The correlator for $j = 0$ is the probability distribution of the molecule's center-of-mass position, i.e., the analog of the incoherent-intermediate scattering function for simple liquids: $\Phi(q00,t) = \Phi_q^s(t)$. Results for $j = 1$ and $j = 2$ deal with the propagation of the dipole- and quadrupole-density fluctuations, respectively. The critical-decay curves, i.e., the solutions for $\varphi = \varphi_c$, organize the bifurcation pattern. They deal with the stretched decay towards the plateaus $f^c(qj0)$. If φ increases above φ_c, the long-time limits $f(qj0) = \Phi(qj0,t \to \infty)$ increase above the plateau because the molecule gets more tightly localized in the frozen solvent. The $f(qj0)$ vs q curves are bell shaped, since the molecules are localized with a nearly Gaussian probability distribution [10]. For $\varphi < \varphi_c$, the correlators exhibit a long-time decay from the plateau to zero, and this is the α process. The α-decay time is larger the smaller the wave vector q, while the α-relaxation stretching increases with increasing q. The q dependence of the relaxation features are similar as observed and explained previously for the tagged-particle correlator $\Phi_q^s(t)$ for simple liquids. Therefore, the following discussion shall be restricted to the $(q = 0)$ limit, i.e., to the reorientational correlators $C^{(j)}(t)$.

Figure 4 exhibits representative decay curves $C^{(j)}(t)$ for the liquid state for two separation parameters, and Fig. 5 exhibits an extended set of susceptibility spectra $\chi^{(j)''}(\omega)$

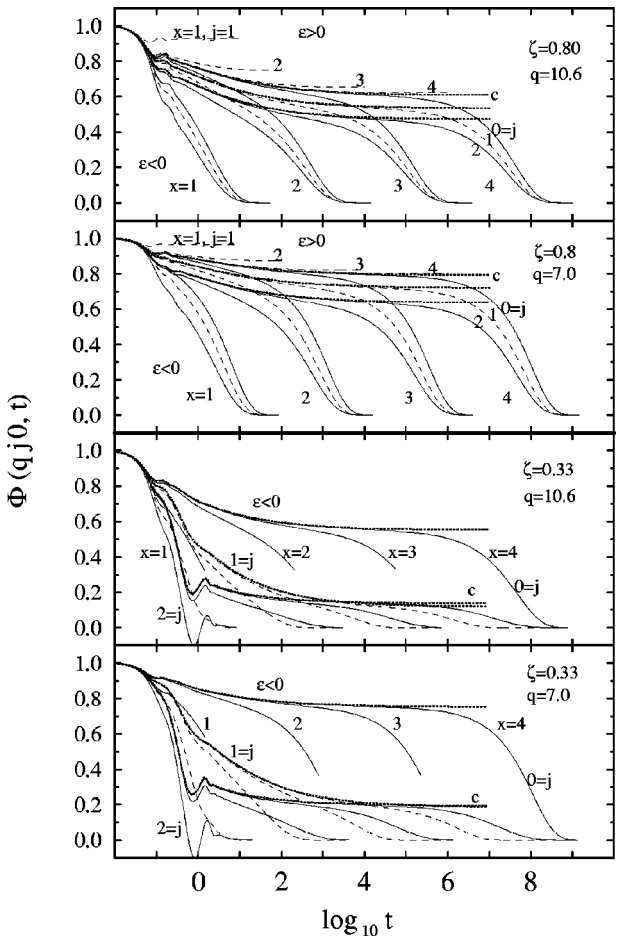

FIG. 3. Correlators Φ for the wave vectors $q=7.0$ and 10.6, elongations $\zeta=0.80$ (upper two panels) and $\zeta=0.33$ (lower two panels), angular indices $j=0,1,2$, and helicity index $\mu=0$ as functions of the logarithm of the time t. The unit of time is chosen here and in all following figures such that the thermal velocity v of the solvent is unity. Correlators are shown as full lines for $j=0,2$ and as dashed lines for $j=1$. The solutions at the critical packing fraction are marked by a c and are shown in dotted lines. The packing fractions are parametrized as $(\varphi-\varphi_c)/\varphi_c=\epsilon=\pm 10^{-x}$, and $x=1,2,3,4$ was chosen. Solutions for the glass states, $\epsilon>0$, are only shown for $\zeta=0.80$, $j=1$. Correlators are truncated where necessary to avoid overcrowding of the figure.

$=\omega C^{(j)''}(\omega)$. The plateaus and critical amplitudes shall be denoted by f_j^c and h_j, respectively. They have been calculated from the mode-coupling functionals [10], and some examples are listed in Table I. These parameters specify the leading-order asymptotic results for the β-relaxation process as explained in Sec. II A for the solvent. The factorization theorem holds in analogy to Eq. (3) [10]:

$$C^{(j)}(t)=f_j^c+h_jG(t). \tag{15}$$

The β-correlator G is the same function as explained in connection with Eqs. (4)–(6) for the solvent. This implies for the critical correlator the asymptotic law

$$C^{(j)}(t)=f_j^c+h_j(t/t_0)^{-a}+\mathcal{O}((t/t_0)^{-2a}); \quad \sigma=0. \tag{16a}$$

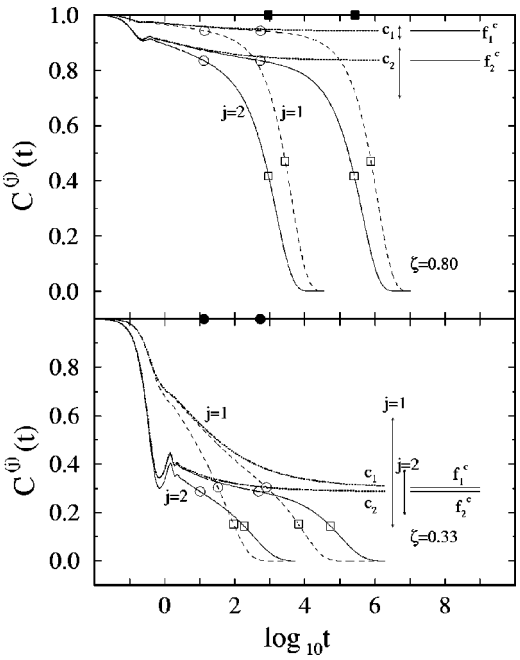

FIG. 4. Reorientational correlators $C^j(t)$ for $j=1$ and $j=2$ for the two elongations $\zeta=0.80$ and $\zeta=0.33$ as function of $\log_{10}t$. The solutions at the critical point are shown in dotted lines and are marked by c_j. The plateau values f_j^c are marked by horizontal lines. The distance parameter is chosen as $\epsilon=(\varphi-\varphi_c)/\varphi_c=-10^{-x}$ with $x=3$ (slower decay) and $x=2$ (faster decay). Open circles and open squares mark the characteristic time scales τ_β^j and τ_α^j for the α and β process, respectively. The full circles and squares mark the time scales 0.704 t_σ, with t_σ from Eq. (6a), and t'_σ from Eq. (6b), respectively. The vertical lines indicate the decay interval described by the asymptotic formulas for the β process (see text, cf. Fig. 7).

The nonergodicity parameter of the glass state, $f_j=C^{(j)}(t\to\infty)$, exhibits the $\sqrt{\sigma}$ singularity

$$f_j=f_j^c+h_j\sqrt{\sigma/(1-\lambda)}+\mathcal{O}(\sigma), \quad \sigma\to 0+, \tag{16b}$$

and the α-process initial decay is given by von Schweidler's law for $t>t_\sigma$ and $\sigma\to 0-$:

$$C^{(j)}(t)=f_j^c[1-(t/\tilde{\tau}_\alpha^j)^b+\mathcal{O}_j((t/\tilde{\tau}_\alpha^j))^{2b}], \qquad \tilde{\tau}_\alpha^j=(f_j^c/h_j)^{1/b}t'_\sigma. \tag{16c}$$

Let us introduce two *ad hoc* time scales for the description of the liquid relaxation outside the transient regime. The center of the β-relaxation process, τ_β^j, shall be defined as the time, where the correlator has decayed to the plateau: $C^{(j)}(\tau_\beta^j)=f_j^c$. The center of the α process shall be defined as the time, where the correlator has decayed to 50% of the plateau: $C^{(j)}(\tau_\alpha^j)=f_j^c/2$. Some values are listed in Table II, and open squares and circles mark these α- and β-relaxation times, respectively, in Fig. 4. The slowing down of the dynamics upon approaching the glass-transition point is reflected by the increase of the time scales with decreasing distance parameter $|\epsilon|$. The two-step scenario emerges, because the ratio of the scales $\tau_\alpha^j/\tau_\beta^j$ increases as well. The α decay leads to the α peaks of the susceptibility spectrum, which are separated from the microscopic excitation peaks

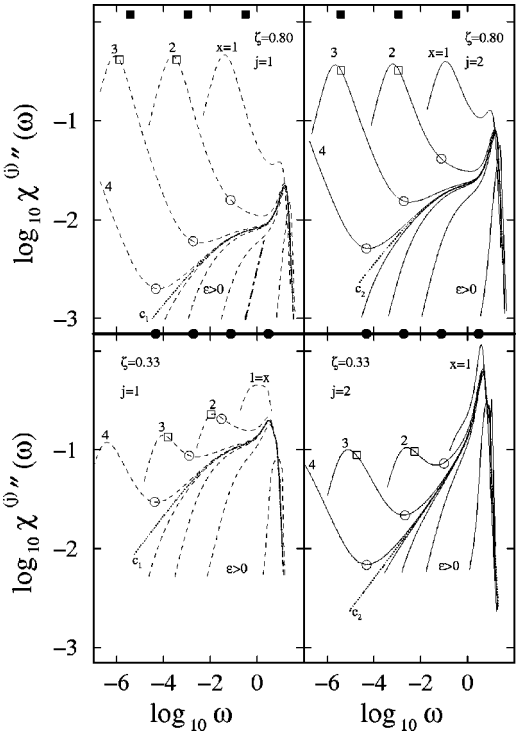

FIG. 5. Double-logarithmic presentation of the susceptibility spectra $\chi^{(j)\prime\prime}(\omega)=\omega C^{(j)\prime\prime}(\omega)$ for angular-momentum indices $j=1$ and $j=2$ for elongations $\zeta=0.80$ and $\zeta=0.33$. Spectra for the critical packing fraction $\varphi=\varphi_c$ are shown in dotted lines and are marked by c_j. The distance parameters are $\epsilon=\pm 10^{-x}$ with x as given in the panels. In the upper left panel, a regular susceptibility spectrum, $\chi''\propto\omega$, corresponding to a white-noise fluctuation spectrum, is indicated by a dashed-dotted straight line of slope unity. The open circles and squares mark the frequencies $1/\tau_\beta^j$ and $1/\tau_\alpha^j$, characterizing the β- and α-relaxation process, respectively. The full circles and full squares mark the frequencies $1/t_\sigma$ and $1/t_\sigma'$, respectively.

by a susceptibility minimum, as is demonstrated in Fig. 5. There, the α-peak-maximum positions, $\omega_{\max}^j$, and the minimum positions, $\omega_{\min}^j$, decrease for $\varphi\to\varphi_c-$. The open squares and circles in Fig. 5 demonstrate, that $\omega_{\max}^j\approx 1/\tau_\alpha^j$ and $\omega_{\min}^j\approx 1/\tau_\beta^j$ as $|\epsilon|\to 0$. The two-step scenario implies that the ratio $\omega_{\max}^j/\omega_{\min}^j$ also decreases upon approaching the glass-transition point. Thus, for $\varphi\to\varphi_c-$, the α peak gets more and more separated from the rest of the spectrum. In this limit, the plateau height is the relative area under the $\chi^{(j)\prime\prime}$ vs $\ln\omega$ curve [16]:

$$f_j^c=\int_{-\infty}^{\ln\omega_{\min}^j}\chi^{(j)\prime\prime}(\omega)\;d\ln\omega\Big/\int_{-\infty}^{\infty}\chi^{(j)\prime\prime}(\omega)\;d\ln\omega. \tag{17}$$

TABLE I. Plateau values f_j^c and critical amplitudes h_j.

	$\zeta=0.80$		$\zeta=0.33$	
j	f_j^c	h_j	f_j^c	h_j
1	0.943	0.13	0.303	1.94
2	0.835	0.35	0.286	0.46
3	0.701	0.55	0.052	0.46
4	0.540	0.68	0.006	0.13

Figure 4 demonstrates that for $t\lesssim 3$ the dynamics deals with oscillatory motion, i.e., with rotations and librations that are influenced by steric hindrance affects. If these effects would lead to some fast decay towards the correlator's long-time limit, one would find a white-noise low-frequency fluctuation spectrum: $C^{(j)\prime\prime}(\omega)\approx C^{(j)\prime\prime}(\omega=0)$. Equivalently, one would obtain a regular low-frequency susceptibility spectrum varying linearly with ω, $\chi^{(j)\prime\prime}(\omega)\propto\omega$, as is indicated schematically by the straight dashed-dotted line in the upper left panel of Fig. 5. A linear susceptibility spectrum is obtained for the glass spectra for $\omega\ll 1/t_\sigma$, since the correlators approach the limit f_j exponentially for $t\gg t_\sigma$. This is shown by the $(\epsilon>0)$ spectra in Fig. 5. Such regular spectra are also found for the low-frequency wings of the α peaks, since the liquid correlators approach zero exponentially for $t\gg\tau_\alpha^j$. At the bifurcation point, however, the critical decay leads to a power-law spectrum which, according to Eq. (16a), reads

$$\chi^{(j)\prime\prime}(\omega)=h_j\sin(a\pi/2)\Gamma(1-a)(\omega t_0)^a+\mathcal{O}((\omega t_0)^{(2a)}). \tag{18}$$

For $t\ll t_\sigma$, the correlators follow the critical decay if $|\sigma|$ is small. Therefore the spectra are approaching the asymptotic ω^a law for $1/t_\sigma\ll\omega\ll 1/t_0$, as is demonstrated for the $(x=4)$ results in Fig. 5. The stretching of the first relaxation step leads to the strong enhancement of the intensity of the spectral minimum $\chi_{\min}^j=\chi^{(j)\prime\prime}(\omega_{\min}^j)$ relative to any possible

TABLE II. Time scales τ_α^j and τ_β^j.

	$\zeta=0.80$		$\zeta=0.33$	
	$x=2$	$x=3$	$x=2$	$x=3$
τ_α^1	2.75×10^3	7.65×10^5	9.29×10^1	6.51×10^3
τ_α^2	9.21×10^2	2.56×10^5	1.85×10^2	5.39×10^4
τ_α^3	4.40×10^2	1.20×10^5	5.98×10^1	4.43×10^3
τ_α^4	2.41×10^2	6.43×10^4	6.55×10^1	1.74×10^4
τ_β^1	1.37×10^1	5.42×10^2	3.33×10^1	8.11×10^2
τ_β^2	1.31×10^1	5.34×10^2	1.03×10^1	4.80×10^2
τ_β^3	1.32×10^1	5.32×10^2	2.53×10^1	7.24×10^2
τ_β^4	1.25×10^1	5.22×10^2	1.00×10^1	4.74×10^2

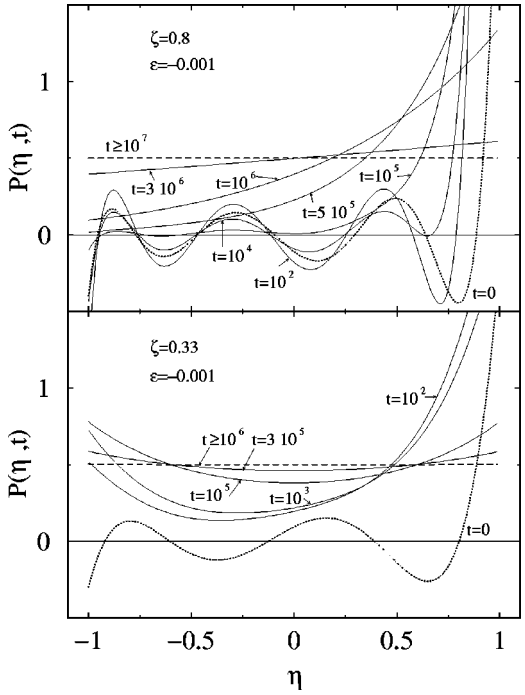

FIG. 6. Evolution of the probability density $P(\eta,t)$ to find at time t the molecular axis $\vec{e}(t)$ with projection $\eta(t)$ onto its initial direction. The dotted lines are the initial distributions, Eq. (19b), downscaled by a factor of 10. The oscillations around $P(\eta,t)=0$ are due to restricting the infinite sum over angular-momentum indices in Eqs. (19) to $j\leqslant 7$ (upper panel) and $j\leqslant 5$ (lower panel), respectively.

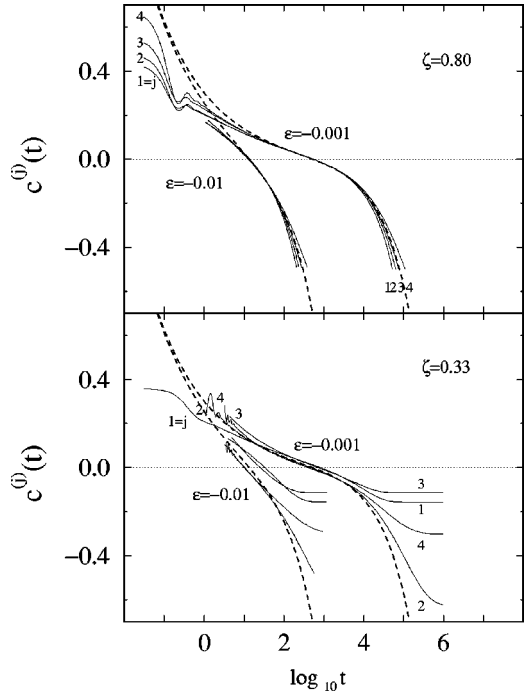

FIG. 7. The full lines exhibit the reorientational correlators rescaled to $c^{(j)}(t)=[C^{(j)}(t)-f_j^c]/h_j$ for two distance parameters ϵ and the angular-momentum indices $j=1-4$. The dashed lines show the β-correlator $G(t)=c_\sigma g_-(t/t_\sigma)$ of the hard-sphere system, obtained from Eqs. (4), (5), and (6a).

estimation of a white-noise-background spectrum. This enhancement also is exhibited by the experimental data reproduced in Fig. 1.

Let us consider the probability density $P(\eta,t)=\langle\delta(\eta(t)-\eta)\rangle$ for the molecule's axis $\vec{e}(t)$ to have the projection $\eta(t)$ on its initial direction $\vec{e}$: $\eta(t)=\vec{e}(t)\vec{e}$. Since $\delta(\eta(t)-\eta)=1/2+\Sigma_{j=1}^{\infty}(j+1/2)P_j(\eta)P_j(\eta(t))$, one gets

$$P(\eta,t)=1/2+\sum_{j=1}^{\infty}(j+1/2)P_j(\eta)C^{(j)}(t). \tag{19a}$$

Thus, knowledge of the set of $C^{(j)}(t)$, $j=1,2,\ldots$, is equivalent to knowing $P(\eta,t)$. If the summation over j is understood with the cutoff l_{co}, Eq. (19a) describes the evolution of the distribution with the initial value

$$P(\eta,t=0)=1/2+\sum_{j=1}^{l_{co}}(j+1/2)P_j(\eta). \tag{19b}$$

Figure 6 exhibits results for the small distance parameter $-\epsilon=(\varphi_c-\varphi)/\varphi_c=0.001$ corresponding to $x=3$. The dotted lines exhibit $P(\eta,t=0)/10$, calculated with $l_{co}=7$ for $\zeta=0.80$, and $l_{co}=5$ for $\zeta=0.33$, respectively. Within the dynamical window, where the leading-order result for the β relaxation, Eq. (15), applies, one gets

$$P(\eta,t)=P^c(\eta)+H(\eta)G(t), \tag{20a}$$

$$P^c(\eta)=1/2+\sum_{j=1}^{\infty}(j+1/2)f_j^cP_j(\eta);$$
$$H(\eta)=\sum_{j=1}^{\infty}(j+1/2)h_jP_j(\eta). \tag{20b}$$

Thus the distribution relaxes towards the distribution $P^c(\eta)$, which is frozen for $\varphi=\varphi_c$. The relaxation does not exhibit any correlation between changes in time described by $G(t)$, and variations with angle described by $H(\eta)$. This is the scenario expected for relaxation due to dephasing in the random distribution of sizes and shapes of the cages producing steric hindrance for the rotations. For $\zeta=0.80$, the β regime extends from $t=10$ to about 10^4 as shown in Fig. 4, and the upper panel of Fig. 6 exhibits the described phenomena for $t=10^2$ and $t=10^4$. The β-relaxation window is somewhat smaller for $\zeta=0.33$, as will be discussed in quantitative detail below in connection with Fig. 7. The dephasing relaxation for this case is demonstrated in Fig. 6 for $t=10^2$ and 10^3.

The beginning of the α-relaxation process follows von Schweidler's law, Eq. (16c). It is identical with the end of the β process, and thus it is described within the scenario based on Eqs. (20). The most drastic difference between large- and small-elongation relaxation shows up for the α process outside the von Schweidler regime. For $\zeta=0.80$, the probability decreases monotonically if the angle Θ of the axis increases from its initial value $\Theta=0$ to $\Theta=\pi$. This is shown in the upper panel of Fig. 6 for $t\geqslant 5\times 10^5$. As time increases, the probability for $\eta\approx 1$ decreases, while it increases for $\eta\approx -1$. Thus, the relaxation towards the equilib-

rium distribution $P(\eta,t=\infty)=1/2$ is similar to what one would expect for diffusion on a sphere. For $\zeta=0.33$, the correlators for odd j decay faster than the corresponding correlators with the even index $(j+1)$. This is demonstrated in Fig. 4 and by the numbers τ_α^j in Table II. Therefore the α process consists of an intermediate time step leading to a probability distribution that is nearly symmetric with respect to the equator $\eta=0$. Only at later times, the symmetric distribution relaxes to the equilibrium distribution. Figure 6 shows that, already for the rather short time $t=10^2$, $P(\eta,t)$ exhibits a minimum. For $t=10^3$, there is an overshooting effect of the probability for $\vec{e}(t)=-\vec{e}$: $P(\eta=-1,t=10^3)>0.5$; and this effect increases if the time increases to $t=10^5$. Thus, the relaxation pattern is that expected for a random process of large-angle flips of the molecule's axis.

B. Dipole vs quadrupole relaxation for strong steric hindrance

The equations for the nonergodicity parameters [10] imply that the f_j increase towards unity if the coupling coefficients in Eq. (12) are increased towards infinity. For this strong-coupling limit, one derives from Eq. (19a) that $P(\eta,t)\to\delta(\eta-1)$. Because of continuity, for strong steric hindrance and for $t<t_\sigma$, $P(\eta,t)$ is a narrowly peaked distribution centered around $\eta\approx 1$. Thus, one expects the expansion coefficients f_j for not too large values of j to form a smoothly decreasing sequence of j: $f_1>f_2>\cdots$, $f_j\approx(f_{j-1}+f_{j+1})/2$. Table I demonstrates this result quantitatively for $\zeta=0.80$ and $\varphi=\varphi_c$:

$$f_1^c>f_2^c>f_3^c>f_4^c, \quad \text{large } \zeta. \tag{21a}$$

In particular, the ratio (f_1^c/f_2^c) of the relative strengths of the α peaks for the dipole relaxation, f_1^c, and for the quadrupole relaxation, f_2^c, is larger than unity. One cannot conclude quantitatively from f_1^c/f_2^c the ratio $\chi_1''(\omega_{\max}^1)/\chi_2''(\omega_{\max}^2)$ of the α-peak heights, since the shapes of the spectra depend on j. However, Fig. 5 demonstrates that the two ratios are close to each other. One can also characterize the α-peak height relative to the microscopic-peak height, $r_j=\chi^{(j)\prime\prime}(\omega_{\max}^j)/\chi^{(j)\prime\prime}(\omega_{\mathrm{mic}}^j)$, or relative to the minimum intensity, $r_j'=\chi^{(j)\prime\prime}(\omega_{\max}^j)/\chi^{(j)\prime\prime}(\omega_{\min}^j)$. From Fig. 5, one infers $r_1/r_2\approx 4$, and $r_1'/r_2'\approx 3$, i.e., the $(j=1)$ vs $(j=2)$ enhancement effect appears even more pronounced.

According to Eq. (16b), the nonergodicity parameters increase with increasing $(\varphi-\varphi_c)$. On the other hand, $1-f_j^c>f_j-f_j^c$. Therefore, h_j must decrease if f_j^c increases, so that the strongly coupled parameters f_j leave the asymptotic regime for Eq. (16b) for similar magnitudes of σ. Table I quantifies this result for $\zeta=0.80$. In particular

$$h_1<h_2, \quad \text{large } \zeta. \tag{21b}$$

The reasoning assumes f_j to be large, and thus it cannot be applied for too large j. There is some j_0, so that h_j decreases with increasing j for $j>j_0$. Within the frequency window, where the leading-order asymptotic law for the critical decay is valid, Eq. (18), one derives an enhancement of the $(j=2)$ spectrum relative to the $(j=1)$ spectrum, since

$$\chi^{(2)\prime\prime}(\omega)/\chi^{(1)\prime\prime}(\omega)=h_2/h_1, \quad 1/t_\sigma\ll\omega\ll 1/t_0. \tag{22}$$

The dotted lines c_1 and c_2 in the upper panels of Fig. 5 demonstrate this result.

For a strongly near- $(\eta=1)$ peaked probability distribution $P(\eta,t)$, one can approximately replace averages of functions of η by the functions of the average $\langle\eta\rangle$. Thus, Lebon *et al.* concluded $f_j=P_j(f_1)$ [28]. Specializing to $\varphi=\varphi_c$, one quantifies the sequence of f_j^c in terms of its first value f_1^c:

$$f_j^c=P_j(f_1^c), \quad \zeta\to\infty. \tag{23a}$$

Substituting into Eq. (16b) and specializing to $\sigma\to 0+$, one can also quantify the sequence of h_j by the first term h_1:

$$h_j=P_j'(f_1^c)h_1, \quad \zeta\to\infty. \tag{23b}$$

From Table I one infers, that for $\zeta=0.80$ the error of Eq. (23a) for $j=2$ (3,4) is as small as 0.1% (3%,7%), and Eq. (23b) is obeyed for $j=2$ (3,4) within 5% (22%,45%).

The strong nonlinear couplings of the structural-relaxation modes require that all correlators enter the first relaxation step, the second relaxation step, and the equilibrium state nearly at the same respective time. This is demonstrated in Fig. 3 for $\zeta=0.80$. The most striking manifestation of the coupling effect occurs at the center of the β-relaxation window for $\sigma\to 0-$. In this case, the factorization theorem, Eq. (15), is valid. All correlators cross their plateau at the same time, say τ_β, where τ_β is the zero of the β-correlator $G(t)$. Because of the scaling law, Eq. (5), one gets the result $\tau_\beta=\hat{t}_-t_\sigma$, i.e.

$$\tau_\beta^j=\hat{t}_-t_\sigma, \quad \sigma\to 0_-. \tag{24}$$

Here, t_σ is the scale from Eq. (6a), and $\hat{t}_-$ is the zero of the master function: $g_-(\hat{t}_-)=0$. For the HSS it reads $\hat{t}_-=0.704$ [17]. The open and full circles in Fig. 4 show that the asymptotic Eq. (24) is obeyed very well for $\zeta=0.80$. Since the α processes of $C^{(1)}(t)$ and $C^{(2)}(t)$ start at the same time $\hat{t}_-t_\sigma$ and reach zero nearly at the same time, one expects from $C^{(1)}(\hat{t}_-t_\sigma)=f_1^c>f_2^c=C^{(2)}(\hat{t}_-t_\sigma)$ that the decay time for $C^{(1)}$ is larger than that for $C^{(2)}$:

$$\tau_\alpha^1>\tau_\alpha^2, \quad \text{large } \zeta. \tag{25}$$

Furthermore, the $C^{(1)}(t)/f_1^c$ vs $\ln t$ plot is somewhat steeper than the corresponding graph for $j=2$. This means that the stretching is larger for the $(j=2)$ α process than for the $(j=1)$ α process. If one interpolates the decay functions by a Kohlrausch law, $C^{(j)}(t)/f_j^c\approx\exp[-(t/\tau_\alpha)^{\beta_j}]$, the stretching exponent for $j=1$ is larger than that for $j=2$:

$$\beta_1>\beta_2, \quad \text{large } \zeta. \tag{26}$$

Stretching can also be quantified by the width w at half-height of the α peak of the susceptibility spectrum. For $\zeta=0.80$ our model yields for $j=1(2,3,4)$, $w=1.16(1.25,1.37,1.50)$ decades. The Kohlrausch processes leading to the same w require stretching exponents $\beta=0.99(0.90,0.82,0.74)$.

The derivation of the inequality for the time scales can be put on a quantitative level by combining Eq. (16c) with the

two inequalities in Eqs. (21). One gets in analogy to Eq. (25): $\tilde{\tau}_\alpha^1 > \tilde{\tau}_\alpha^2$. The α-relaxation law for the $C^{(j)}(t)$ holds in analogy to Eq. (7): $C^{(j)}(t) = \tilde{C}_j(\tilde{t})$. If the shape function $\tilde{C}_j(\tilde{t})/f_j^c$ would be independent of j, the ratio $\tau_\alpha^1/\tau_\alpha^2$ would be equal to the ratio $\tilde{\tau}_\alpha^1/\tilde{\tau}_\alpha^2 = [f_1^c h_2 / h_1 f_2^c]^{1/b}$. But the latter is about 2.1 times larger than $\tau_\alpha^1/\tau_\alpha^2$.

C. Dipole vs quadrupole relaxation for weak steric hindrance

There are two universal phenomena that are relevant for a discussion of the dynamics for weak steric hindrance. The first one concerns the limit $\zeta = 0$ of the center-of-mass correlator $\Phi(j=0,\ \mu=0,q,t) = \Phi_q^s(t)$, which is identical to the tagged-particle-density correlator of the larger of the two spheres forming the dumbbell. If the radius of this sphere, say d_1, is of the same order or larger than the radius d of the solvent spheres, the steric hindrance is very effective. In this case, $\Phi_q^s(t)$ exhibits the canonical bifurcation scenario if φ crosses φ_c, as was discussed comprehensively in Ref. [18]. This implies that for $d_1 \gtrsim d$ the $(j=0)$ correlators exhibit only a smooth ζ dependence for ζ decreasing to zero. A side remark shall be added to this conclusion. If the ratio of the diameters d_1/d of a sphere moving in a glass of hard spheres decreases towards zero, there occurs a percolation transition at some critical value (d_1^c/d). This is a type-A transition, i.e., a bifurcation where the Lamb-Mössbauer factor decreases continuously to zero for $(d_1 - d_1^c)$ approaching zero from above [15,16]. Because of continuity, it is obvious that for a dumbbell built of sufficiently small spheres, $d_1 < d_1^c$, there will be a type-A transition if the elongation ζ decreases to some critical value $\zeta^* > 0$. If ζ crosses ζ^*, the dynamics changes from one dealing with molecules localized in the hard-sphere glass to one dealing with delocalized molecular motion. This small-ζ phenomenon for small molecules is not considered in this paper.

The second universal phenomenon deals with a type-A transition resulting from the fact, that for top-down symmetrical molecules the MCT equations of motion of the even-j correlators decouple from the odd-j ones [10,26]. The even-j correlators couple to the function $\Phi_q^s(t)$, and thus the conventional transition scenario of this correlator enforces the same for all other correlators with even j. However, such coupling does not exist for odd j. For large ζ, this results in no considerable effect. But all coupling coefficients in the equations of motion approach zero for odd j if ζ tends to zero. Consequently, for all $\varphi > \varphi_c$ there is some critical elongation $\zeta_c(\varphi)$ for a type-A transition. For the studied model $\zeta_c(\varphi) < \zeta_c(\varphi_c) = 0.296$ [10,14]. Choosing ζ sufficiently close to $\zeta_c(\varphi)$, it can happen that for odd j, $f_j < f_{j+1}$ or even $f_j < f_{j+3}$ [10]. The transition at $\zeta_c(\varphi)$ shall not be studied in this paper. For the demonstration of the small- $(\zeta - \zeta_c(\varphi_c))$ phenomena, the value $\zeta = 0.33$ has been chosen so large that the canonical sequence for the plateau values in the $(q=0)$ limit, Eq. (21a), is not violated, as is quantified in Table I. But it is chosen so small, that the precursor effects of the type-A transition seriously influence the results for the dumbbell dynamics. Thereby, the results are also representative for such cases, where the type-A transition singularity is avoided [15] due to a weak breaking of the top-down symmetry of the solvent-solute interaction.

The even-j correlators show the conventional behavior. Therefore, the discussion of their trends with decreasing ζ for fixed j can be held analogously to that given in Sec. III B for the trends with increasing j for fixed large ζ. Thus one understands that the $(j=2)$ α process for $\zeta = 0.33$ is weaker, faster, and more stretched than that for $\zeta = 0.80$, as it is demonstrated in Figs. 4 and 5. The half-width of the α peak for $j = 2(4)$ is $w = 1.66(1.86)$ decades as for a Kohlrausch process with exponent $\beta = 0.67(0.59)$. Notice in particular from Fig. 4, that the β-relaxation scale τ_β^2 for the $x=3$ result is close to the ζ- and j-independent number $\hat{t}_- t_\sigma$ from Eq. (24). For $x=2$, the asymptotic formula is obeyed reasonably, but the preasymptotic corrections are larger for $\zeta = 0.33$ than for $\zeta = 0.80$.

The most obvious precursor of the type-A transition is the suppression of the plateau values f_j for odd j. This leads to a violation of the rule $(f_1 + f_3)/2 \approx f_2$, as is quantified in Table I. The general qualitative reasoning from Sec. III B explains, that the suppression of f_1 is connected with an enhancement of h_1: $h_1(\zeta = 0.33)/h_1(\zeta = 0.80) \approx 15$. The amplitude h_1 is given by the resolvent of the so-called stability matrix, and at a type-A transition the resolvent exhibits a pole [15,16]. Hence $h_1(\zeta \to \zeta_c(\varphi))/h_2(\zeta \to \zeta_c(\varphi)) \to \infty$, and the regular trend, Eq. (21b), is reversed:

$$h_1 > h_2, \quad \text{small } \zeta. \tag{27}$$

For our example one infers from Table I that $h_1/h_2 \approx 4.2$. According to Eq. (22), the critical spectrum for the dipole relaxation is considerably larger than that for the quadrupole relaxation, as is demonstrated by the dotted lines in the lower two panels of Fig. 5.

Combining Eq. (27) with von Schweidler's law, Eq. (16c), one concludes that the $C^{(1)}(t)$ vs $\ln t$ curve crosses its plateau f_1^c much steeper than the $C^{(2)}(t)$ vs $\ln t$ curve. This is illustrated in the lower panel of Fig. 4. Hence the α relaxation of the $(j=1)$ response is faster than the one of the $(j=2)$ response:

$$\tau_\alpha^1 < \tau_\alpha^2, \quad \text{small } \zeta. \tag{28}$$

Again the order for large ζ, Eq. (25), is reversed. From Table II, one infers for $x=3$, $\tau_\alpha^1/\tau_\alpha^2 = 0.12$. Accordingly, the α-peak positions for the $(x=3)$ spectra for $j=1$ and $j=2$ in the lower panels of Fig. 5 differ by about one order of magnitude. For the ratio of the von Schweidler scales in Eq. (16c), one gets $\tilde{\tau}_\alpha^1/\tilde{\tau}_\alpha^2 = [h_2 f_1^c / h_1 f_2^c]^{1/b} \to 0$ for $\zeta \to \zeta_c$, and this identifies the smallness of the ratio τ^1/τ^2 as a precursor of the type-A transition. The preceding discussion is valid more generally and explains that all the odd-j correlators decay faster than the nearby even-j ones. As a result, the probability distribution $P(\eta,t)$ approaches first an even function of η, before the equilibrium value 0.5 is obtained, as is demonstrated in the lower panel of Fig. 6.

D. β-relaxation scaling

The factorization theorem for the β relaxation, Eq. (15), means that the rescaled correlators $c^{(j)}(t) = (C^{(j)}(t) - f_j^c)/h_j$ are given independently from j by the β-correlator $G(t)$ of the solvent. The latter obeys the scaling law, specified by

Eqs. (4)–(6a). For fixed rescaled time $\hat{t}=t/t_\sigma$, the cited formulas deal with the results correctly up to order $\sqrt{|\sigma|}$ [16]. The leading corrections are of order $|\sigma|$, and they explain the range of validity of the leading results for separations ϵ [17]. Figure 7 demonstrates these statements. On a 10% accuracy level the leading-order results describe 4%(18%;45%;20%) of the decay of the correlators around the plateau for $\zeta=0.80$, $j=1(\zeta=0.80, j=2; \zeta=0.33, j=1; \zeta=0.33, j=2)$. These decay intervals are indicated in Fig. 4 by vertical lines. For $\epsilon=-0.001$, the corresponding dynamical window extends from about $t=10$ to about 10^5, while it extends from about $t=3$ to about $t=100$ for $\epsilon=-0.01$. This discussion requires a reservation: The corrections to the scaling results can lead to such a violation of Eq. (24), which appears as an offset of the plateau [17]. This offset can be noted in the lower panel of Fig. 7 for the odd-j results. The good description of the β decay of the ($\zeta=0.33$) results for odd j holds only after a correction of the offset. For $t\gtrsim 10^4$, the correction effects cause the $c^{(j)}(t)$ for $\zeta=0.80$ to differ from $G(t)$; one infers from Fig. 7 that the $c^{(j)}(t)$ increase with increasing j. The general results for the theory of the corrections imply that then also $c^{(j)}(t)$ increases with j for $t\lesssim 10$ [17]. The $c^{(j)}(t)$ vs $\ln t$ curves do not intersect for $\hat{t}_- t_\sigma$ but they touch each other as is demonstrated in the upper panel of Fig. 7. Corresponding results also hold for $\zeta=0.33$ after the mentioned offset is eliminated.

Equations (5) and (15) lead to the scaling law for the susceptibility spectra: $\chi^{(j)''}(\omega)/h_j = c_\sigma \hat{\chi}_\pm(\omega t_\sigma)$. The master spectra $\hat{\chi}_\pm(\hat{\omega})=\hat{\omega} g''_\pm(\hat{\omega})$ are given by the Fourier-cosine transform $g''_\pm(\hat{\omega})$ of the master functions $g_\pm(\hat{t})$. The master spectrum for the glass state describes the crossover from a regular spectrum for small rescaled frequencies, $\hat{\chi}_+(\hat{\omega}\ll 1) \propto \hat{\omega}$, to the critical spectrum at large rescaled frequencies, $\hat{\chi}_+(\hat{\omega}\gg 1)\propto \hat{\omega}^a$. It deals with the knee exhibited by the spectra for $\epsilon>0$ and $x=3,4$ in Fig. 5. The master spectrum for the liquid describes the crossover from the von Schweidler high-frequency tail of the α peak, $\hat{\chi}_-(\hat{\omega}\ll 1)\propto 1/\hat{\omega}^b$, to the critical decay for large rescaled frequencies, $\hat{\chi}_-(\hat{\omega}\gg 1) \propto \hat{\omega}^a$. The results describe in the small-σ limit the β-relaxation minimum as it can be seen in Fig. 5 for the $x=3$ and $x=4$ results. In particular, the factorization theorem explains why the spectral minima $\omega_{\min}$ are located at the same position independently of j and ζ. The leading-order formulas imply $\omega_{\min}=\hat{\omega}_{\min}/t_\sigma$, where $\hat{\omega}_{\min}$ denotes the minimum of the master spectrum $\hat{\chi}_-$. For the hard-sphere system, one gets $\hat{\omega}_{\min}=1.56$ [17].

Obviously, the β-relaxation scaling laws can describe the susceptibility minimum only for such small distance parameters, for which $\omega_{\min}$ is located in that frequency window where the ($\sigma=0$) spectrum exhibits the asymptotic ω^a law, Eq. (18). Figure 5 shows that for the model under study this window is restricted to $\omega<0.01$. This means, that $\omega_{\min}$ has to be located about three decades below the peak of the microscopic susceptibility spectrum. For $\omega>0.01$, the critical spectrum is modified by crossover effects to the transient dynamics. The susceptibility minimum with $\omega_{\min}>0.01$ is due to the crossover of the α-peak tail to the microscopic excitation spectrum; it cannot be discussed by the universal asymptotic laws for the MCT bifurcation. One concludes from Fig. 5, that $|\epsilon|<10^{-2}$ needs to be satisfied in order to apply the β-scaling laws for the model under study.

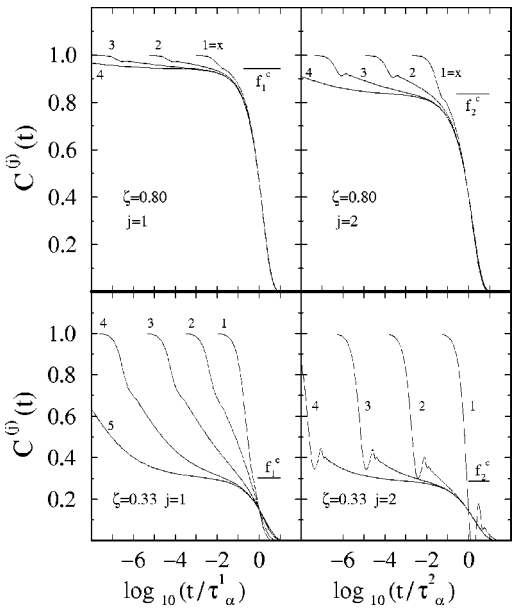

FIG. 8. Reorientational correlators $C^j(t)$ for $j=1,2$ and $\zeta=0.80$ and $\zeta=0.33$ for various distance parameters $\epsilon=-10^{-x}$, presented as functions of $\log_{10}(t/\tau^j_\alpha)$. The α-relaxation-time scale τ^j_α is defined by $C^{(j)}(\tau^j_\alpha)=f^c_j/2$. The horizontal lines indicate the plateaus f^c_j.

E. α-relaxation scaling

The α-relaxation scaling law reads for the reorientational correlators in analogy to Eq. (7):

$$C^{(j)}(t)=\tilde{C}_j(\tilde{t}), \quad \tilde{t}=t/t'_\sigma. \tag{29}$$

The ϵ-independent master function $\tilde{C}_j$ obeys as initial condition the von Schweidler law: $\tilde{C}^{(j)}(\tilde{t})=f^c_j-h_j\tilde{t}^b+\mathcal{O}(\tilde{t}^{2b})$. The superposition principle for the susceptibility spectra reads $\chi^{(j)''}(\omega)=\tilde{\chi}^{(j)''}(\tilde{\omega})$ with $\tilde{\omega}=\omega t'_\sigma$ denoting the rescaled frequency. The ϵ-independent master spectrum is given by the Fourier-cosine transform of the master correlators $\tilde{\chi}^{(j)''}(\tilde{\omega})=\tilde{\omega}\tilde{C}^{(j)''}(\tilde{\omega})$. Consequently, the above-defined α-relaxation time scales τ^j_α and susceptibility maximum positions $\omega^j_{\max}$ read

$$\tau^j_\alpha=\tilde{t}^j t'_\sigma, \quad \omega^j_{\max}=\tilde{\omega}^j/t'_\sigma, \tag{30}$$

where $\tilde{t}^j$ is defined by $\tilde{C}^{(j)}(\tilde{t}^j)=f^c_j/2$ and $\tilde{\omega}^j$ denotes the peak frequency of $\tilde{\chi}^{(j)''}(\tilde{\omega})$. The scaling law implies that a representation of $C^{(j)}(t)$ as a function of the rescaled time t/τ^j_α should superimpose correlators for different distance parameters ϵ on the common curve $\tilde{C}^{(j)}(\tilde{t}/\tilde{t}^j)$. Asymptotic validity means that the $\ln(t/\tau^j_\alpha)$ interval, where the scaling law is obeyed, expands to arbitrary size for $\epsilon\to 0$. A corresponding statement holds for the representation of the susceptibility peaks as functions of the rescaled frequency. The corrections to the leading-order asymptotic laws are larger, the larger the critical amplitude h_j is [17,18]. Figures 5 and 8

demonstrate that the described scenario for the evolution of the α process is valid for $\zeta=0.80$, and also for $\zeta=0.33$ in the case $j=2$. For strong steric hindrance, the α-scaling law works for larger values of $(\varphi_c-\varphi)$, than the β-scaling law. This is so, because the leading corrections to the α-scaling law are of relative size $\mathcal{O}(|\epsilon|)$, while they are of relative size $\mathcal{O}(\sqrt{|\epsilon|})$ for the β-scaling law [17].

Figure 8 demonstrates a drastic $(j=1)$ vs $(j=2)$ effect of the α scaling for $\zeta=0.33$. The dipole correlators do not exhibit the superposition principle for $|\epsilon|>10^{-4}$, nor do the correlators for the other odd values of j. For $j=1$ the plateau emerges only for extremely small values of the distance parameter $|\epsilon|\leqslant 10^{-4}$. The α-peak heights of the dipole spectra decrease with decreasing $|\epsilon|$ in Fig. 5 in contradiction to the scaling-law prediction. This anomaly is caused by the large size of the critical amplitude h_1, which was explained in connection with Eq. (27). More precisely, it is caused by the large percentage of the decay of $C^{(1)}(t)$ described by the β-scaling law as is indicated by the vertical lines in Fig. 4. To formulate this observation quantitatively, let us remember that the decay of the correlator near the plateau is described by Eqs. (5), (6), and (15): $C^{(j)}(t)=f_j^c+h_j\sqrt{|\sigma|}g_-(t/t_\sigma)$. The master function $g_-(\hat{t})$ for small positive values and all negative ones is well approximated by $\hat{g}(\hat{t})=-B\hat{t}^b+B_1/(B\hat{t}^b)$. Here, B_1 is determined by the exponent parameter λ and for our solvent model reads $B_1=0.431$ [17]. Thus one gets for $C^{(j)}(t)\lesssim f_j^c$ within the window for the validity of the β-relaxation scaling law:

$$C^{(j)}(t)=f_j^c-\sqrt{|\sigma|}h_j\{B(t/t_\sigma)^b-B_1/[B(t/t_\sigma)^b]\}. \tag{31a}$$

The leading corrections to this formula can explain the possible offset of f_j^c or, equivalently, of the scales t_σ [17], which was noticed above in connection with Fig. 7 for $\zeta=0.33$. Equation (31a) can be rewritten as $C^{(j)}(t)=[f_j^c-h_j\tilde{t}^b]+h_j|\sigma|B_1/\tilde{t}^b$. Here, the bracket is the α-scaling-law description of the initial part of the α process, and the term proportional to B_1 is the leading correction. The correction term to the α-scaling law deals with that part of the β process below the plateau, which is not given by the von Schweidler's large-$\hat{t}$ asymptote. Therefore, one can write that for the α process for not too large values of rescaled time $\tilde{t}$:

$$C^{(j)}(t)=\tilde{C}^{(j)}(\tilde{t})+h_j|\sigma|B_1/\tilde{t}^b. \tag{31b}$$

The analog of this formula was shown in Ref. [17] to describe the evolution of the α process of the density correlators of the HSS perfectly for $|\epsilon|\leqslant 0.1$. It was also shown that the corresponding spectrum describes the susceptibility peak to increase above the scaling-law constant $\tilde{\chi}''(\tilde{\omega}_{\max})$ if the separation $|\epsilon|$ increases from 10^{-2} to 10^{-1}.

In Fig. 9, the evolution of the $(j=1)$ α process for small steric hindrance is reexamined. Instead of rescaling the time with the *ad hoc* scale τ_α^1, the theoretically motivated scale t'_σ is chosen. One recognizes, that the found scenario does not exhibit any qualitative peculiarity anymore, compared to what is presented in Fig. 8 for $\zeta=0.33$ and $j=2$. The $(j=1)$ vs $(j=2)$ anomaly is identified as an anomaly of the size of the corrections only. In the case of the small elongation, the distance parameter $|\epsilon|$ has to be taken almost two orders of magnitude smaller for $j=1$ in order to render the corrections to the α scaling as small as found for $j=2$. For $|\epsilon|\gtrsim 10^{-3}$, even including the leading corrections to von Schweidler's law, one can explain the relaxation from the plateau only up to some offset in the time scale. This is demonstrated in Fig. 9 by the dotted lines for $x=2,3$.

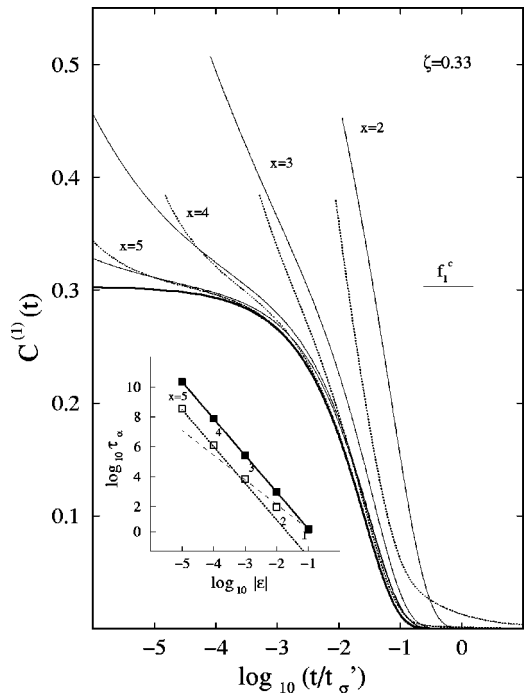

FIG. 9. Dipole correlator $C^{(1)}(t)$ of the dumbbell with small elongation $\zeta=0.33$ and distance parameters $\epsilon=-10^{-x}$ for $x=2-5$ as functions of the logarithm of the rescaled time $\tilde{t}=t/t'_\sigma$ (light full lines). Here t'_σ is the second critical time scale, Eq. (6b). The heavy full line is the α-relaxation master function $\tilde{C}^{(1)}(\tilde{t})$. The dotted lines show the leading-order α-scaling result plus the leading correction term according to Eq. (31b). The inset exhibits in a double-logarithmic plot t'_σ (full squares) and the *ad hoc* scaling time τ_α^1 (open squares) for $x=1-5$. The full straight line with slope $\gamma=2.46$ exhibits the power-law formula for the hard-sphere system, Eq. (6b). The dashed line interpolates the open squares for $x=1,2,3$ with an effective power-law exponent $\gamma'=1.65$, while the dotted line is the asymptotic small-ϵ result for τ_α^1.

Two remarks concerning tests of the second scaling law shall be added. The definition of the time scale τ_α^j used in Fig. 8 was arbitrary. Let us consider more general definitions to be parametrized by a number $k>1$ and denoted as τ_k. The subscripts α and j shall be dropped for the sake of simplicity, and the definition shall be $C^{(j)}(\tau_k)=f_j^c/k$. If the scaling law is valid, one finds in analogy to Eq. (30) $\tau_k=\tilde{t}_k t'_\sigma$. Here, $\tilde{t}_k$ is defined by $\tilde{C}^{(j)}(\tilde{t}_k)=f_j^c/k$. In this case, the choice of k is irrelevant, since the ratio of two different scales is ϵ independent, $\tau_{k_1}/\tau_{k_2}=\tilde{t}_{k_1}/\tilde{t}_{k_2}$. However, if preasymptotic corrections are present, the scales are not equivalent. The range of validity of the superposition principle expands from large to small rescaled times. This follows from Eq. (31b) and is demonstrated in Fig. 9. One gets for $k_1<k_2$,

$$\tau_{k_1}/\tilde{t}_{k_1} < \tau_{k_2}/\tilde{t}_{k_2} < t'_\sigma \tag{32}$$

For a detection of the superposition principle for an as large as possible value of $|\epsilon|$, one should therefore choose an as large as possible value of k for the rescaling procedure. Thereby, the artificial crossing point of the rescaled curves at $t=\tau_k$ is suppressed as much as possible. Otherwise, one introduces a time scale τ_k for the characterization of a decay process that cannot be characterized by a single scale. The outcome of this ill-defined procedure is demonstrated in the lower left panel in Fig. 8. In this case, $\tau_\alpha^1=\tau_{k=2}$ is a parameter extracted from the correlator which, according to Fig. 7, is adequately specified by the two scales c_σ and t_σ of the β-relaxation scaling law. The dashed line in the inset of Fig. 9 demonstrates explicitly that the scale τ_α^1 does not exhibit the asymptotic behavior for $|\epsilon| \geqslant 10^{-3}$. The asymptotic law $\tau_\alpha^1=\tilde{t}_2 t'_\sigma$ is followed only for $\epsilon \leqslant 10^{-4}$.

The second remark concerns the determination of the exponent γ entering the power-law behavior for the α-relaxation time scale, as specified by Eqs. (6b) and (30). These results are based on the validity of the scaling law [16]. Therefore, one cannot appeal to MCT if one fits power laws for scaling times for cases where the scaling law is violated. The dashed line in the inset in Fig. 9 demonstrates that the scale τ_α^1 for $|\epsilon| \geqslant 10^{-3}$ can be fitted well by a power law for a two-decade variation of the distance parameter $|\epsilon|$. The identified effective exponent $\gamma' < \gamma$ describes the variation of τ_α^1 over three orders of magnitude; but nevertheless γ' has no well-defined meaning for the discussion of our model.

IV. CONCLUSIONS

Solving the MCT equations of motion for the dynamics of a hard-sphere dumbbell moving in a hard-sphere liquid, first-principle results have been obtained for the evolution of the glassy dynamics of the reorientational degrees of freedom of a molecule. It was found that one has to distinguish between two scenarios, namely, between strong steric hindrance as found for large elongations ζ of the dumbbell, and weak steric hindrance as found for small elongations.

For strong steric hindrance, the mode-coupling coefficients for the reorientational degrees of freedom in Eq. (12) are of the same order as the ones entering Eq. (2) for the description of the translational degrees of freedom of the solvent. The dependence of the various parameters on the angular-momentum index j is similar to the dependence on the wave vector q. One has to view $j(j+1)$ as the analog of q^2. While the q dependence reflects the decomposition of the direct solute-solvent correlations in plane waves, the j-dependence reflects the decomposition in spherical harmonics. Hence one finds that all reported results on the j dependence of the reorientational correlators $C^{(j)}(t)$ are similar—and can be explained in a similar manner—as known from the previous work on the tagged-particle-density correlators $\Phi_q^s(t)$ in simple liquids [18,29]. In particular, it was shown that with increasing j the α-peak-strength parameters f_j^c, Eq. (21a), the α-relaxation-time scales τ_α^j, Eq. (25), and the stretching exponents β_j, Eq. (26), decrease. These findings reproduce qualitatively the three general differences between dielectric-loss and depolarized-light-scattering spectra, which were discussed in Sec. I in connection with Fig. 1. Because of Eq. (1a), the relaxation of the correlator Φ follows that of the kernel m. Therefore, the α-relaxation time scale of the $(q \to 0)$ density fluctuations, say τ_α^0, is larger than the corresponding scale of the longitudinal elastic modulus $m_{q=0}(z)$, say τ_α^m. For strong steric hindrance, the decay of the cage is the prerequisite for the reorientation of the molecule, and therefore $\tau_\alpha^0 < \tau_\alpha^2$. Thus one expects the fourth general feature of the α relaxation listed in the Introduction: $\tau_\alpha^2/\tau_\alpha^m > 1$. For our model one gets for $\epsilon=-0.01$, $\tau_\alpha^m=130$, $\tau_\alpha^0=240$, $\tau_\alpha^2=920$. The ratio $\tau_\alpha^2/\tau_\alpha^m \approx 7$ is of the same order as cited in Sec. I for PC and Salol.

The mode-coupling coefficients in Eq. (12) decrease to zero if j tends to infinity. Thus the solutions for large j are sums of many small terms, which are not strongly correlated. Each term exhibits the short-time von Schweidler law behavior for the α relaxation $C^{(j)}(t)-f_j^c \propto (t/t'_\sigma)^b$. Therefore, one expects for $C^{(j)}(t)$ the characteristic function of the stable Lévy distribution $\exp[(-t\Gamma_j)^b]$ [3]. For the density correlators of the solvent, Fuchs has worked out the limit behavior for the α-relaxation master function for $q \to \infty$ and showed how the Kohlrausch law with $\beta=b$ arises [30]. We suspect that a similar derivation can be done for the reorientational correlators. Therefore, we conjecture that the sequence of Kohlrausch exponents $\beta_1 > \beta_2 > \beta_3 > \cdots$ converges towards the von Schweidler exponent b. Molecular-dynamics-simulation data for a model of water have been interpreted consistently within the standard MCT scenario [31–33]. In particular, $C^{(j)}(t)$ exhibits conventional behavior [34]. One concludes that water exhibits strong-steric-hindrance effects. Therefore it is reassuring that the sequence of the first five Kohlrausch exponents β_j decreases with increasing j monotonously towards the von Schweidler exponent [35]. A further general result, namely, the increase in the initial part of the series of critical amplitudes, Eq. (21b), is also found in the simulation data for $j \leqslant 3$ [35].

Figure 1 exhibits as full lines the $(j=1)$ and $(j=2)$ spectra calculated for $\zeta=0.80$. The lines for $x=1$ and $x=2$ are the ones discussed in Fig. 5, and the other two refer to $x=1.33$ and $x=1.67$, respectively. In order to transfer the MCT results, which are calculated with *ad hoc* units specified in Sec. II, to the units used by the experimentalists, one has to introduce three scales. The first and second scale transfer the calculated dimensionless normalized spectra $\chi^{(j)''}(\omega)$ for $j=1$ and $j=2$ to the units used by the experimentalists for their dielectric-loss and depolarized-light-scattering spectra, respectively. The third scale shifts our frequency scale to the GHz scale. In the double-logarithmic representation, the first two scales define an overall vertical shift of the diagrams in Fig. 5, while the third scale defines a horizontal shift of the figures. Intending to compare data for PC for different temperatures with the MCT results for different packing fractions φ, one gets a mapping of the T scale onto the φ scale via Eq. (9). The result is shown as an inset in Fig. 1. The inset also includes the point with coordinates of the critical packing fraction of the solvent φ_c and the critical temperature $T_c=180$ K. This value for T_c was determined for PC by analyzing neutron scattering data [36], and has recently been corroborated in an MCT analysis of vari-

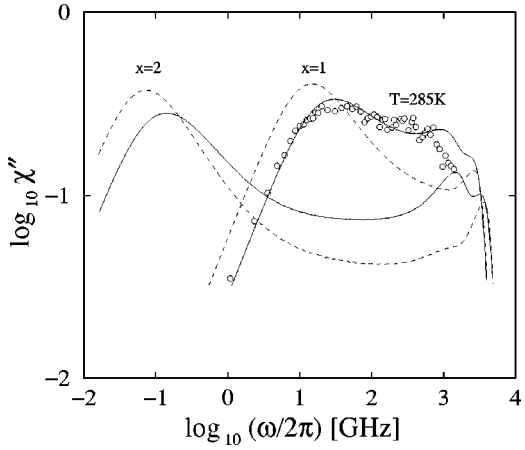

FIG. 10. Susceptibility spectrum χ'' of PC as measured by incoherent neutron scattering [38] for $q=1.3$ Å^{-1} and $T=285$ K (circles). The solid lines exhibit the neutron-scattering response of the discussed MCT model, and the dashed lines are the mere center-of-mass contributions for packing fractions corresponding to $x=1$ and 2. The computational wave vector is $q=7.4$. As done in Fig. 1, a rescaling of the theoretical frequencies by a factor of 10 was chosen to match the scale of the experiment. The normalized theoretical spectra have been rescaled by a factor of 1.1.

ous other PC experiments [37]. Our results in Fig. 1 describe the evolution of the two types of PC spectra semiquantitatively. In particular, the extrapolation of the T-φ relation yields a reasonable estimation of the critical temperature for that system, which is demonstrated through the dashed line in the inset. There is no obvious reason why the studied dilute solution of hard symmetric dumbbells in a hard-sphere solvent should produce spectra, which are similar to the data for PC. We consider the found similarities to a large extent as accidental. The theoretical curves are added in Fig. 1 with the mere intention to justify the conclusion: the model studied in this paper and our choice of parameters are relevant for achieving an understanding of experiments in glass-forming molecular liquids.

In order to further corroborate the preceding conclusion, let us consider Fig. 10. The data points exhibit a susceptibility spectrum of PC measured by incoherent-neutron-scattering spectroscopy for the wave vector $q=1.3$ Å^{-1} [38]. A remarkable feature of the α-peak spectrum compared to the spectra shown in Fig. 1 is that it is less pronounced relative to the spectrum of the microscopic excitation band and that it is more stretched. The two dashed lines in Fig. 10 exhibit the spectra for the center-of-mass correlator $\Phi_q^s(t)=\Phi(q,j=0,\mu=0,t)$ for $q=7.4$ in order to emphasize that this leading approximation for the scattering function cannot easily explain the experimental findings. The shown α peaks of Φ_q^s have a half-width of $w=1.34$ decades as produced by a Kohlrausch process with exponent $\beta=0.84$. The scattering function $F_q(t)$ is a sum over the contributions of the molecule's constituents and hence it is a superposition of the density correlators for all angular-momentum indices j. For the symmetric dumbbell one gets up to some normalization constant [10]

$$F_q(t)=\sum_j (2j+1)\ b_j(q\zeta/2)^2\Phi(q,j,0,t), \qquad (33)$$

where $b_j(z)$ are the spherical Bessel functions. The full lines in Fig. 10 exhibit the spectra for $F_q(t)$ for $q=7.4$. The α peaks have a half-width of $w=1.61$ decades as produced by a Kohlrausch law with stretching exponent $\beta=0.69$. The frequency was rescaled as explained in connection with Fig. 1 and the scale for the spectra was adjusted to meet the one of the data. Comparison of the full line with the dashed one for $x=2$ shows the features distinguishing the α processes of $F_q''(\omega)$ from that of $\Phi_q^{s\,\prime\prime}(\omega)$. The result calculated for $x=1$ shows that the finding for our model semiquantitatively accounts for the α-peak data.

Some side remarks considering the comparisons in Figs. 1 and 10 might be useful. A schematic-model analysis of the PC data gave the exponent parameter $\lambda\approx 0.75$ [37], in good agreement with the values found from analyses of the susceptibility minima with the β-relaxation scaling laws [19,20,38]. The value is close to the result $\lambda\approx 0.74$ for the hard-sphere system, Eq. (8). This accident ensures that the master function for the susceptibility minimum and the values of all anomalous exponents of PC agree within the experimental uncertainties with the corresponding quantities of the model studied in this paper; and this is a prerequisite of a successful fit. Accidently, the ratio of the α-relaxation times $\tau_\alpha^1/\tau_\alpha^2$ noted in Table II for $\zeta=0.8$ is only a bit larger than the ratio of the α-peak-maximum positions of PC, $\omega_{\max}^2/\omega_{\max}^1$, exhibited in Fig. 1; and this is another request for a reasonable fit. Since the ratio decreases with decreasing ζ, some $\zeta<0.80$ could be chosen to reproduce the specified $(j=1)$ vs $(j=2)$ effect quantitatively. Nevertheless, it is remarkable that the fit in Fig. 1 reproduces the ratios of α-peak maximum intensity to β-minimum intensity $\chi^{(j)\prime\prime}(\omega_{\max})/\chi^{(j)\prime\prime}(\omega_{\min})$ reasonably well for both values of j. Neither is it trivial that the model reproduces reasonably the $(j=1)$ vs $(j=2)$ effect for stretching.

A new liquid-glass-transition scenario is predicted which is referred to as the regime of weak steric hindrance for reorientational motion. It is characterized by $(j=1)$ vs $(j=2)$ effects, more generally by odd-j vs even-j effects, which are qualitatively different from the results described above as strong-steric-hindrance results. The new scenario occurs if precursor phenomena of a type-A-transition between two nonergodic states strongly influence the asymptotic results for the conventional MCT bifurcation. The scenario appears if the particle interactions deviate not too strongly from spherical symmetry, e.g., if a linear molecule exhibits only small deviations from a top-down symmetry and if there are not too large elongations. Six features characterize the weak-steric-hindrance scenario. First (i), the plateaus f_j^c for the reorientational correlators for odd j are suppressed in comparison to what one would expect by interpolating or extrapolating the values for nearby even-j plateaus (Table I). Most importantly (ii), the critical amplitude h_1 is larger than h_2, Eq. (27), so that the canonical ordering of the h_j for small j, Eq. (21b), is reversed. Third (iii), the percentage of the decay of the reorientational correlators $C^{(j)}(t)$, which can be explained by the leading- plus next-to-leading-order asymptotic formulas for the β relaxation is larger for $j=1$ than for $j=2$; as is indicated by the vertical lines in Fig. 4. The structural relaxation of the reorientations is dominated by large-angle flips (iv), as shown in Fig. 6

for the dumbbell with elongation $\zeta=0.33$. The α-relaxation-time scale for $j=1$ is smaller than for $j=2$, Eq. (28), (v) so that the canonical order of the α-relaxation scales, Eq. (25), is reversed. This can cause the $C^{(j)}(t)$ vs $\ln t$ graphs for $j=1$ to cross the graphs for $j=2$, as is shown for the $\zeta=0.33$ results in Figs. 3 and 4. Finally (vi), for distance parameters $|\epsilon|\geqslant 10^{-3}$, where the conventional $C^{(j)}(t)$ vs $\ln t/(\tau_\alpha^j)$ plot exhibits the α-relaxation scaling law for $j=2$, the correlators for $j=1$ do not show the validity of the superposition principle, as is demonstrated in Fig. 8. Nor does the scale τ_α^1, defined as the time for a 50% decay of the α-relaxation correlator, exhibit the power-law behavior with the correct exponent γ as is shown in the inset of Fig. 9.

A side remark concerning a molecular-dynamics study of the evolution of glassy dynamics in a Lennard-Jones dumbbell liquid by Kämmerer *et al.* [39–41] might be in order. It was reported that the correlators dealing with translational degrees of freedom and also for the ones for the reorientational dynamics for angular index $j\neq 1$ could be interpreted qualitatively within the universal asymptotic MCT formulas. However, the evolution of the dipole correlators did not fit into the standard MCT pattern. It was found that $h_1>h_2$ and $\tau_\alpha^1<\tau_\alpha^2$. A drastic violation of the α-scaling law was noted quite similar to what is exhibited in the lower left panel of Fig. 8. The scale τ_α^1 exhibited a deviation from the asymptotic law $\epsilon^{-\gamma}$, but a fit by $\tau_\alpha\propto\epsilon^{-\gamma'}$ with γ' as discussed in the inset of Fig. 9 was possible. These simulation results for $j=1$ differ from those for water simulations [32–35] as well as from the experimental findings for propylene carbonate quoted in Fig. 1. However, they agree with the features (ii), (v), and (vi) specified in the preceding paragraph. Moreover, the property (iv) concerning the large-angle flips is also obtained in Ref. [39]. Accidently, the $x=2$ results in the lower panel of Fig. 5 show that the minimum position of the $j=1$ spectrum exceeds that of the $j=2$ spectrum by nearly one order of magnitude, in agreement with the corresponding finding in Ref. [41]. Furthermore, the α-peak variation with x shown in the lower left panel of Fig. 5 is in qualitative agreement with that reported in Ref. [39]. In view of these observations it does not seem impossible that the scenario studied in Refs. [39–41] fits into the framework of the ideal MCT. However, it is not clear whether or not the results of Refs. [39–41] can be explained by our theory for type-A precursors of a dilute solution of molecules. First, the simulation results for the dumbbell liquid do not exhibit a particular decrease of f_1^c relative to f_2^c. Second, the β-relaxation scaling has not been documented for the dumbbell liquid and so it is unclear whether or not the feature (iii) holds for that case.

Summarizing, it shall be emphasized that all qualitative features for the evolution of the structural relaxation studied in this paper have been explained by means of the formulas for the leading-asymptotic expansions and their leading-order-correction formulas for the bifurcation scenario. In this sense, these asymptotic formulas can be considered as the essence of MCT. However, in order to explain the characteristic ($j=1$) vs ($j=2$) differences for the relaxation patterns, it is necessary to also understand the general trends of the nonuniversal parameters with variations of wave-vector q and angular-momentum index j. And this requires the use of MCT as a microscopic theory based on the knowledge of the equilibrium structure.

ACKNOWLEDGMENTS

We thank the authors of Refs. [19,20,38] for the permission to use their data files and M. Fuchs for many stimulating discussions. We kindly thank F. Sciortino for permission to cite his unpublished simulation results for the reorientational dynamics of water. We gratefully acknowledge helpful critique and suggestions for improvements of the manuscript written to us by H.Z. Cummins, R. Pick, and R. Schilling. This work was supported by Verbundprojekt BMBF 03-G05TUM.

[1] E. Leutheusser, Phys. Rev. A **29**, 2765 (1984).
[2] U. Bengtzelius, W. Götze, and A. Sjölander, J. Phys. C **17**, 5915 (1984).
[3] W. Götze and L. Sjögren, Rep. Prog. Phys. **55**, 241 (1992).
[4] W. van Megen and S. M. Underwood, Phys. Rev. E **47**, 248 (1993).
[5] W. van Megen, Transp. Theory Stat. Phys. **24**, 1017 (1995).
[6] T. Gleim, W. Kob, and K. Binder, Phys. Rev. Lett. **81**, 4404 (1998).
[7] T. Gleim and W. Kob, Eur. Phys. J. B **13**, 83 (2000).
[8] W. Götze, J. Phys.: Condens. Matter **11**, A1 (1999).
[9] R. Schilling and T. Scheidsteger, Phys. Rev. E **56**, 2932 (1997).
[10] T. Franosch, M. Fuchs, W. Götze, M. R. Mayr, and A. P. Singh, Phys. Rev. E **56**, 5659 (1997).
[11] L. Fabbian, A. Latz, R. Schilling, F. Sciortino, P. Tartaglia, and C. Theis, Phys. Rev. E **60**, 5768 (1999).
[12] C. Theis and R. Schilling, J. Non-Cryst. Solids **235-237**, 106 (1998).
[13] L. Fabbian, R. Schilling, F. Sciortino, P. Tartaglia, and C. Theis, Phys. Rev. E **58**, 7272 (1998).
[14] T. Franosch and A. P. Singh, J. Non-Cryst. Solids **235-237**, 150 (1998).
[15] T. Franosch and W. Götze, J. Phys.: Condens. Matter **6**, 4807 (1994).
[16] W. Götze, in *Liquids, Freezing and Glass Transition*, edited by J.-P. Hansen, D. Levesque, and J. Zinn-Justin (North-Holland, Amsterdam, 1991), p. 287.
[17] T. Franosch, M. Fuchs, W. Götze, M. R. Mayr, and A. P. Singh, Phys. Rev. E **55**, 7153 (1997).
[18] M. Fuchs, W. Götze, and M. R. Mayr, Phys. Rev. E **58**, 3384 (1998).
[19] U. Schneider, P. Lunkenheimer, R. Brand, and A. Loidl, Phys. Rev. E **59**, 6924 (1999).
[20] W. M. Du, G. Li, H. Z. Cummins, M. Fuchs, J. Toulouse, and L. A. Knauss, Phys. Rev. E **49**, 2192 (1994).
[21] J. Wuttke, J. Hernandez, G. Li, G. Coddens, H. Z. Cummins, F. Fujara, W. Petry, and H. Sillescu, Phys. Rev. Lett. **72**, 3052 (1994).
[22] P. Lunkenheimer, A. Pimenov, M. Dressel, Yu. G. Goncharov,

R. Böhmer, and A. Loidl, Phys. Rev. Lett. **77**, 318 (1996).
[23] C. Dreyfus, M. J. Lebon, H. Z. Cummins, J. Toulouse, B. Bonello, and R. M. Pick, Phys. Rev. Lett. **69**, 3666 (1996); **76**, 1763(E) (1996).
[24] J.-P. Hansen and I. R. McDonald, *Theory of Simple Liquids*, 2nd ed. (Academic Press, London, 1986).
[25] T. Franosch, W. Götze, M. R. Mayr, and A. P. Singh, J. Non-Cryst. Solids **235-237**, 71 (1998).
[26] A. P. Singh, Ph.D. thesis, TU München, Herbert Utz Verlag, München, 1999.
[27] T. Franosch and A. P. Singh, J. Chem. Phys. **107**, 5524 (1997).
[28] M. J. Lebon, C. Dreyfus, Y. Guissani, R. M. Pick, and H. Z. Cummins, Z. Phys. B: Condens. Matter **103**, 433 (1997).
[29] M. Fuchs, I. Hofacker, and A. Latz, Phys. Rev. A **45**, 898 (1992).
[30] M. Fuchs, J. Non-Cryst. Solids **172-174**, 241 (1994).
[31] P. Gallo, F. Sciortino, P. Tartaglia, and S.-H. Chen, Phys. Rev. Lett. **76**, 2730 (1996).
[32] F. Sciortino, P. Gallo, P. Tartaglia, and S.-H. Chen, Phys. Rev. E **54**, 6331 (1996).
[33] F. Sciortino, L. Fabbian, S.-H. Chen, and P. Tartaglia, Phys. Rev. E **56**, 5397 (1997).
[34] L. Fabbian, F. Sciortino, and P. Tartaglia, J. Non-Cryst. Solids **235-237**, 325 (1998).
[35] F. Sciortino (private communication).
[36] L. Börjesson, M. Elmroth, and L. Torell, Chem. Phys. **149**, 209 (1990).
[37] W. Götze and Th. Voigtmann, Phys. Rev. E **61**, 4133 (2000).
[38] J. Wuttke, M. Ohl, M. Goldammer, S. Roth, U. Schneider, P. Lunkenheimer, R. Kahn, B. Ruffĺe, and R. Lechner, Phys. Rev. E **61**, 2730 (2000).
[39] S. Kämmerer, W. Kob, and R. Schilling, Phys. Rev. E **56**, 5450 (1997).
[40] S. Kämmerer, W. Kob, and R. Schilling, Phys. Rev. E **58**, 2131 (1998).
[41] S. Kämmerer, W. Kob, and R. Schilling, Phys. Rev. E **58**, 2141 (1998).